JEM Journal of Experimental Medicine

ARTICLE

Human *PIK3R1* mutations disrupt lymphocyte differentiation to cause activated PI3Kδ syndrome 2

Tina Nguyen[1,2*], Anthony Lau[1,2*], Julia Bier[1,2*], Kristen C. Cooke[3], Helen Lenthall[1], Stephanie Ruiz-Diaz[1], Danielle T. Avery[1], Henry Brigden[1], David Zahra[1], William A Sewell[1,2], Luke Droney[4], Satoshi Okada[5], Takaki Asano[5], Hassan Abolhassani[6,7], Zahra Chavoshzadeh[8], Roshini S. Abraham[9], Nipunie Rajapakse[10], Eric W. Klee[11], Joseph A. Church[12,13], Andrew Williams[14,15,20], Melanie Wong[14,15,16], Christoph Burkhart[17], Gulbu Uzel[18], David R. Croucher[1,2], David E. James[3,19], Cindy S. Ma[1,2,14], Robert Brink[1,2], Stuart G. Tangye[1,2,14], and Elissa K. Deenick[1,2,14]

Heterozygous loss-of-function (LOF) mutations in *PIK3R1* (encoding phosphatidylinositol 3-kinase [PI3K] regulatory subunits) cause activated PI3Kδ syndrome 2 (APDS2), which has a similar clinical profile to APDS1, caused by heterozygous gain-of-function (GOF) mutations in *PIK3CD* (encoding the PI3K p110δ catalytic subunit). While several studies have established how *PIK3CD* GOF leads to immune dysregulation, less is known about how *PIK3R1* LOF mutations alter cellular function. By studying a novel CRISPR/Cas9 mouse model and patients' immune cells, we determined how *PIK3R1* LOF alters cellular function. We observed some overlap in cellular defects in APDS1 and APDS2, including decreased intrinsic B cell class switching and defective Tfh cell function. However, we also identified unique APDS2 phenotypes including defective expansion and affinity maturation of *Pik3r1* LOF B cells following immunization, and decreased survival of *Pik3r1* LOF pups. Further, we observed clear differences in the way *Pik3r1* LOF and *Pik3cd* GOF altered signaling. Together these results demonstrate crucial differences between these two genetic etiologies.

Introduction

Class IA phosphatidylinositol 3-kinases (PI3Ks; hereafter referred to as PI3K) are a family of heterodimers composed of a catalytic subunit (either p110α, p110β or p110δ, encoded by *PIK3CA*, *PIK3CB*, or *PIK3CD*, respectively) paired with one of several regulatory subunits (p85α, p55α, p50α, which are all encoded by *PIK3R1*; or p85β, p55γ, encoded by *PIK3R2* and *PIK3R3*, respectively; Bilanges et al., 2019; Fruman et al., 2017). PI3K plays key roles in cellular function including proliferation, metabolism, survival, and differentiation (Okkenhaug, 2013). Indeed, PI3K is activated downstream of many receptors important for regulating immune cell activation and differentiation, including the T and B cell antigen receptors (TCR/BCR), costimulatory molecules (e.g., CD40, CD28), cytokine receptors, and TLRs (Bier and Deenick, 2022; Thouenon et al., 2021).

The critical role of PI3K in immune regulation and immune cell function is evidenced by the identification of individuals with heterozygous gain-of-function (GOF) mutations in *PIK3CD* or loss-of-function (LOF) mutations in *PIK3R1* who develop a range of clinical manifestations including recurrent bacterial respiratory infections, susceptibility to herpes virus infections, lymphoproliferation, autoimmunity, enteropathy, and lymphoma (Angulo et al., 2013; Brodsky and Lucas, 2021; Deau et al., 2014; Elkaim et al., 2016; Jamee et al., 2019; Lucas et al., 2014a; Lucas et al., 2014b). Due to similarities in clinical phenotypes

[1]Garvan Institute of Medical Research, Darlinghurst, Australia; [2]School of Clinical Medicine, Faculty of Medicine and Health, University of New South Wales Sydney, Kensington, Australia; [3]Charles Perkins Centre, School of Life and Environmental Sciences, University of Sydney, Sydney, Australia; [4]Department of Clinical Immunology, Royal Brisbane and Women's Hospital, Brisbane, Australia; [5]Department of Pediatrics, Graduate School of Biomedical and Health Sciences, Hiroshima University, Hiroshima, Japan; [6]Department of Biosciences and Nutrition, Division of Clinical Immunology, Karolinska University Hospital Huddinge, Karolinska Institutet, Stockholm, Sweden; [7]Research Center for Immunodeficiencies, Children's Medical Center, Tehran University of Medical Sciences, Tehran, Iran; [8]Pediatric Infections Research Center, Mofid Children's Hospital, Shahid Beheshti University of Medical Sciences, Tehran, Iran; [9]Department of Pathology and Laboratory Medicine, Nationwide Children's Hospital, Columbus, OH, USA; [10]Department of Pediatric and Adolescent Medicine, Division of Pediatric Infectious Diseases, Mayo Clinic, Rochester, MN, USA; [11]Center for Individualized Medicine, Mayo Clinic, Rochester, MN, USA; [12]Division of Clinical Immunology and Allergy, Children's Hospital of Los Angeles, Los Angeles, CA, USA; [13]Keck School of Medicine, University of Southern California, Los Angeles, CA, USA; [14]Clinical Immunogenomics Research Consortium Australasia, Sydney, Australia; [15]Children's Hospital at Westmead, Westmead, Australia; [16]Faculty of Medicine, University of Sydney, Sydney, Australia; [17]Novartis Institutes for Biomedical Research, Novartis Pharma AG, Basel, Switzerland; [18]Laboratory of Clinical Immunology and Microbiology, National Institutes of Allergy and Infectious Diseases, National Institutes of Health, Bethesda, MD, USA; [19]School of Medical Sciences, University of Sydney, Sydney, Australia; [20]Central Clinical School, University of Sydney, Sydney, Australia.

*T. Nguyen, A. Lau, and J. Bier contributed equally to this paper. Correspondence to Elissa K. Deenick: e.deenick@garvan.org.au; Stuart G. Tangye: s.tangye@garvan.org.au.

and aberrant PI3K signaling, the immune dysregulatory conditions resulting from *PIK3CD* GOF or *PIK3R1* LOF mutations have been termed activated PI3Kδ syndrome 1 (APDS1) and APDS2, respectively.

In APDS1, *PIK3CD* GOF mutations directly result in hyperactivation of p110δ (Angulo et al., 2013; Lucas et al., 2014a). In APDS2, the *PIK3R1* LOF mutations affect splice donor or acceptor sites and lead to in-frame skipping of exon 11 and deletion of amino acids 434–475 of p85α, which comprise part of the inter-SH2 domain shared by the p85α, p55α, and p50α isoforms (Deau et al., 2014; Jamee et al., 2019; Lucas et al., 2014b). This mutant protein lacks regulatory function, thereby indirectly resulting in increased activity of the p110δ catalytic subunit (Deau et al., 2014; Lucas et al., 2014b).

Significant advances have been made in determining the molecular and cellular defects underlying altered function of both B and T cells due to heterozygous *PIK3CD* GOF mutations (Al Qureshah et al., 2021; Angulo et al., 2013; Avery et al., 2018; Bier et al., 2019; Cannons et al., 2018; Edwards et al., 2019; Jia et al., 2021; Lau et al., 2020; Lucas et al., 2014a; Preite et al., 2018a; Preite et al., 2018b; Stark et al., 2018; Wentink et al., 2018; Wray-Dutra et al., 2018). However, far less is known about the effects of heterozygous *PIK3R1* LOF mutations on cell behavior. While it is largely assumed that these will overlap with *PIK3CD* GOF, *PIK3R1* is more widely expressed than *PIK3CD* and can also interact with p110α and p110β, indicating likely differences in mechanisms of disease and cell function. Indeed, APDS2 patients have higher rates of failure to thrive and neurodevelopmental delay than APDS1 patients (Elkaim et al., 2016; Jamee et al., 2019; Maccari et al., 2018), suggesting there are p110δ-independent effects of *PIK3R1* LOF mutations. Thus, to elucidate cellular mechanisms of immune dysfunction and disease pathogenesis in APDS2 patients, it is important to determine the exact effect of *PIK3R1* LOF mutations on B and T cell development, differentiation, and function.

Here, we have performed detailed analyses of lymphocytes from patients with *PIK3R1* LOF mutations as well as generated a novel mouse model of *Pik3r1* LOF with a CRISPR-engineered heterozygous in-frame exon 11 skipping mutation analogous to APDS2 patients. Our findings have revealed intrinsic defects in both B and T cell differentiation due to *PIK3R1* LOF. While some of these defects, such as reduced Ig class switching in B cells, mirrored defects observed in *PIK3CD* GOF cells, others, such as decreased survival at birth and decreased affinity maturation of antigen-specific B cells, were unique to *PIK3R1* LOF. Thus, *PIK3R1* LOF mutations lead to a distinct range of cellular defects, providing a potential explanation for some of the differences in clinical phenotype observed between APDS1 and APDS2 patients.

Results

Increased PI3K signaling due to *PIK3R1* mutations alters human B cell development and differentiation

To determine how *PIK3R1* LOF mutations affect immune cell development, we assessed the lymphocyte compartment of APDS2 patients compared to healthy donors, and as well as to our previously published data from APDS1 patients with *PIK3CD* GOF mutations (Avery et al., 2018). Our cohort comprised 11 *PIK3R1* LOF patients from 8 families (age range 4–39 yr, median 12 yr). Pathogenic *PIK3R1* mutations and clinical features of these patients are listed in Table S1. Seven patients had one of the previously described single nucleotide missense variants that alter the splice donor site of exon 11, affecting exon splicing (Deau et al., 2014; Jamee et al., 2019; Lucas et al., 2014b). In contrast, a novel deletion variant (c.1300-35_1302del) was found in the related patients 1–4. This variant also resulted in skipping of exon 11, as shown by production of a shorter product following PCR amplification of cDNA corresponding to the relevant region of mRNA transcript (Fig. S1 A).

The percentage of B cells in *PIK3R1* LOF patients was significantly decreased compared to healthy donors (Fig. 1 A). Within the B cell compartment, *PIK3R1* LOF patients had a higher frequency of transitional B cells, and a concurrent reduction in frequencies of the more mature subsets, i.e., naïve and memory B cells, compared with healthy donors (Fig. 1 B). These perturbations to the B cell pool in *PIK3R1* LOF patients recapitulated our previous observations for *PIK3CD* GOF patients (Fig. 1 B; Avery et al., 2018). Increased PI3K signaling due to *PIK3CD* GOF mutations has been shown to inhibit class switching (Avery et al., 2018). Thus, we assessed proportions of memory B cells expressing IgG or IgA. *PIK3R1* LOF patients had fewer IgG^+ memory cells than healthy donors, whereas proportions of IgA^+ memory B cells were not statistically different between patients and healthy donors (Fig. 1 C). In contrast, *PIK3CD* GOF patients had significant reductions of both IgG^+ and IgA^+ memory B cells compared to healthy donors (Fig. 1 C; Avery et al., 2018).

PIK3CD GOF mutations compromise human B cell development in the bone marrow (BM), with an impediment at the pre-BII stage, resulting in marked reductions in mature B cells in BM (Avery et al., 2018; Dulau Florea et al., 2017). To examine the impact of increased PI3K signaling due to *PIK3R1* LOF mutations on early B cell development, and link this to the accumulation of transitional B cells in the periphery, we examined the BM of APDS2 patients. While we were only able to obtain BM aspirates from two patients, the data clearly shows that, similar to *PIK3CD* GOF, *PIK3R1* LOF patients exhibited disrupted B cell development, with a contracted population of mature BM B cells compared to healthy donors (Fig. 1 D; and Fig. S1, B and C). However, our data suggested that in *PIK3R1* LOF patients this was accompanied by an increase in pro-B, rather than the increase in pre-BII cells we previously observed in *PIK3CD* GOF patients (Fig. 1 D and Fig. S1, B and C). The block in B cell development observed in APDS1 and APDS2 was much milder than that observed in patients with X-linked agammaglobulinemia due to mutations in *BTK*, where >90% of B cells are arrested at the pro-B cell stage (Fig. 1 D).

PIK3R1 LOF mutations disrupt human peripheral T cell subsets

Next, we explored the impact of *PIK3R1* LOF mutations on T cell differentiation. While the total frequency of $CD3^+$ T cells in most patients was comparable to healthy donors (Fig. S1 D), there were reduced proportions of $CD4^+$ T cells, along with a modest increase in $CD8^+$ T cells in *PIK3R1* LOF patients compared to healthy controls (Fig. 1 E).

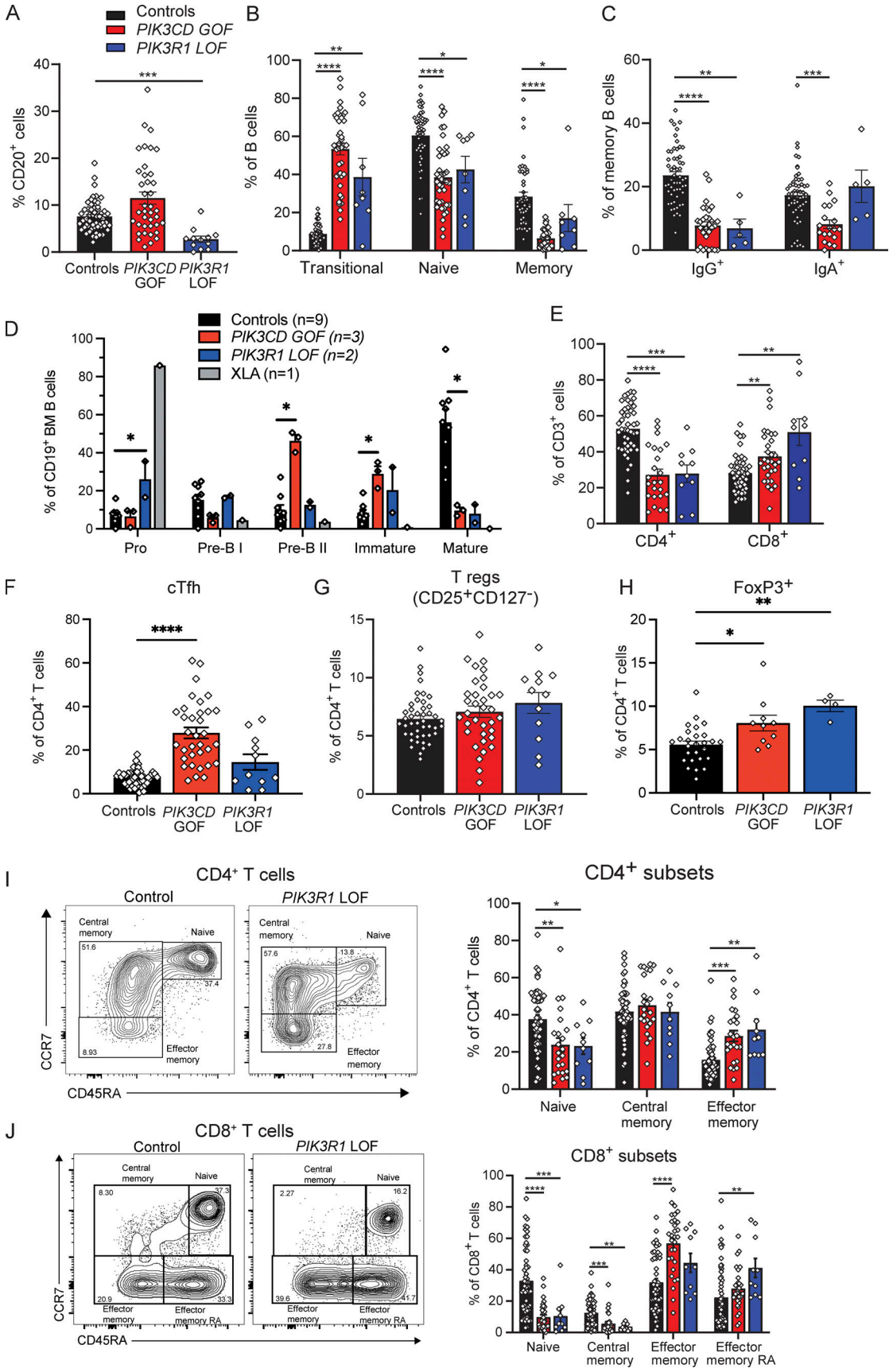

Figure 1. **Phenotype of lymphocytes in *PIK3R1* LOF patients. (A–D)** PBMCs from healthy donors (n = 46–55) and *PIK3R1* LOF patients (n = 5–11) were stained to determine the proportions of (A) B cells ($CD20^+$); (B) transitional ($CD10^+CD27^-$), naïve ($CD10^-CD27^-$), and memory ($CD10^-CD27^+$) B cells; (C) IgG^+ or

IgA$^+$ switched memory B cells; (D) mononuclear cells isolated from BM aspirates from healthy donors (n = 9), *PIK3R1* LOF (n = 2), *PIK3CD* GOF (n = 3), and X-linked agammaglobulinemia (XLA; n = 1) patients were stained to identify distinct B cell subpopulations. **(E–H)** Frequencies of BM B cell subsets are shown. PBMCs were stained to determine the proportions of (E) CD4$^+$ or CD8$^+$ T cells; (F) Tfh cells; and (G) Tregs defined as CD127^{lo}CD25^{hi} and (H) Total FoxP3$^+$ cells. **(I and J)** Proportions of naïve (CD45RA$^+$CCR7$^+$), T_{CM} (CD45RA$^-$CCR7$^+$), T_{EM} (CD45RA$^-$CCR7$^-$) and/or effector memory cells re-expressing CD45RA (CD45RA$^+$CCR7$^-$) within the (I) CD4$^+$ T cell compartment and (J) CD8$^+$ T cell compartment were determined. Points show each individual analyzed as well as mean ± SEM and include previously published data for *PIK3CD* GOF patients (n = 19–39; Avery et al., 2018; Bier et al., 2019; Edwards et al., 2019), except FoxP3 staining which has not been published before. Statistical significance was determined by Kruskal–Wallis test, *P < 0.05, **P < 0.01, ***P < 0.001, ****P < 0.0001.

Analysis of the CD4$^+$ T cell compartment revealed that approximately half of the *PIK3R1* LOF patients had increased proportions of circulating T follicular helper (cTfh; CD45RA$^-$CXCR5$^+$) cells (Fig. 1 F). This did not associate with the age of the patients, nor *PIK3R1* mutation (Fig. S1 E). However, in contrast to *PIK3CD* GOF patients, the overall cTfh population was not significantly different between *PIK3R1* LOF patients and healthy donors (Fig. 1 F). Despite this, *PIK3R1* LOF cTfh and non-Tfh memory subsets expressed higher levels of programmed cell death protein-1 (PD-1) relative to healthy donors, indicative of higher levels of activation and/or exhaustion (Fig. S1 F). Neither *PIK3CD* GOF nor *PIK3R1* LOF patients had increased proportions of regulatory T cells (Tregs), as defined by a CD127^{lo}CD25^{hi} surface phenotype (Fig. 1 G). They did show an increased number of total FOXP3$^+$ cells (Fig. 1 H). However, within the FOXP3$^+$ population, *PIK3R1* LOF patients had fewer CD25$^+$ cells, compared to healthy donors suggesting that these cells were not bona fide Tregs (Fig. S1 G).

Within the CD4$^+$ T cell compartment, proportions of naïve cells were significantly decreased and effector memory (T_{EM}) cells significantly increased in patients with *PIK3R1* LOF mutations, compared to healthy donors (Fig. 1 I). The *PIK3R1* LOF CD8$^+$ T cell compartment also contained increased proportions of cells corresponding to later stages of differentiation, i.e., terminally differentiated effector memory cells expressing CD45RA, together with a paucity of naïve and central memory (T_{CM}) cells (Fig. 1 J). The depletion of naïve T cells, and skewing of CD4$^+$ and CD8$^+$ T cells in *PIK3R1* LOF patients toward terminal differentiation, is a phenocopy of the T cell compartment in *PIK3CD* GOF patients (Fig. 1, H and I; Bier et al., 2019; Edwards et al., 2019). Lastly, we quantified functional Th subsets defined by differential expression of CXCR3 and CCR6 (Acosta-Rodríguez et al., 2007; Ma et al., 2015; Morita et al., 2011). It has previously been shown that *PIK3CD* GOF patients have an increase in the CXCR3$^+$ Tfh1 population (Bier et al., 2019; Preite et al., 2018a). In contrast, in *PIK3R1* LOF patients the distribution of Th1, Th17, Th1/Th17, and Th2-type subsets among both memory and cTfh cells was similar to healthy donors (Fig. S1, H–J). We also examined NK cells in *PIK3R1* LOF patients and observed no difference in total proportions of NK cells, nor in the CD56^{bright} or CD56^{dim} populations (Fig. S1 K).

Generation of a mouse model of APDS2

While patients with APDS2 displayed striking alterations in lymphocyte subsets, it can be difficult to determine whether these changes are intrinsic effects of the mutation or result from infections and/or treatments the patients have experienced. Thus, to further investigate the direct intrinsic effects of *PIK3R1* LOF mutations on immune cell development independently of confounding extrinsic factors, we generated a mouse model. In more than 80% of cases, APDS2 results from a heterozygous variant at the −1, +1 or +2 nucleotide of the splice donor site of exon 11, which causes skipping of exon 11 and deletion of amino acids 434–475 of p85α (Deau et al., 2014; Jamee et al., 2019; Lucas et al., 2014b). Using CRISPR/Cas9 gene editing, a G > C base substitution was introduced into the exon 11 splice donor site of *Pik3r1*, referred to here as *Pik3r1* LOF. As expected, this resulted in transcripts that lacked exon 11 and encoded p85α of lower molecular weight (Fig. S2, A–C). Unexpectedly, heterozygous *Pik3r1* LOF mice did not show normal Mendelian ratios at weaning (Fig. S2, D and E), suggesting *Pik3r1* LOF affected the viability of fetal or neonatal mice. In contrast, no change in Mendelian ratios of *Pik3cd* GOF mice was observed (Fig. S2, D and E). To verify that the *Pik3r1* LOF mutation resulted in increased PI3K signaling, we assessed phosphorylation of S6, which is induced in response to PI3K activation, in follicular B cells. We observed increased pS6 expression in both *Pik3r1* LOF and *Pik3cd* GOF B cells compared to WT B cells (Fig. S2 F). This was largely due to an increase in the percentage of cells that had upregulated pS6 expression. Interestingly, levels of pS6 were modestly but significantly higher in unstimulated follicular B cells from *Pik3r1* LOF mice than from *Pik3cd* GOF mice (Fig. S2 F).

Lymphocyte populations in *Pik3r1* LOF mice

Having established that our mouse model replicated the alterations in the p85α subunit and PI3K signaling observed in APDS2 patients, we assessed how the *Pik3r1* LOF mutation affected B and T cell development. An ∼2-fold increase in proportions of pro-B cells was the only significant difference found between populations of developing B cells in BM of *Pik3r1* LOF and WT mice (Fig. S2, G–I). This mirrored our observations for disrupted B cell development in *PIK3R1* LOF patients, where we found an accumulation of pro-B cells in BM (Fig. 1 D and Fig. S1 C). Notably however, this contrasted B cell development in *PIK3CD* GOF patients and *Pik3cd* GOF mice, which was typified by increased proportions of pre-B and immature cells, and significantly decreased mature B cells (Fig. S2, G–I).

In the periphery, *Pik3cd* GOF mice had increased numbers of splenic B cells compared to WT mice, however, this was not observed in *Pik3r1* LOF mice (Fig. 2 A). Further, *Pik3r1* LOF mice did not display the alterations in transitional B cell populations and decrease in percentages of mature B cells seen in *Pik3cd* GOF mice (Fig. 2, B–D). In contrast, *Pik3r1* LOF did disrupt the mature B cell compartment, evidenced by decreased follicular B cells and increased splenic marginal zone B cells in *Pik3r1* LOF mice

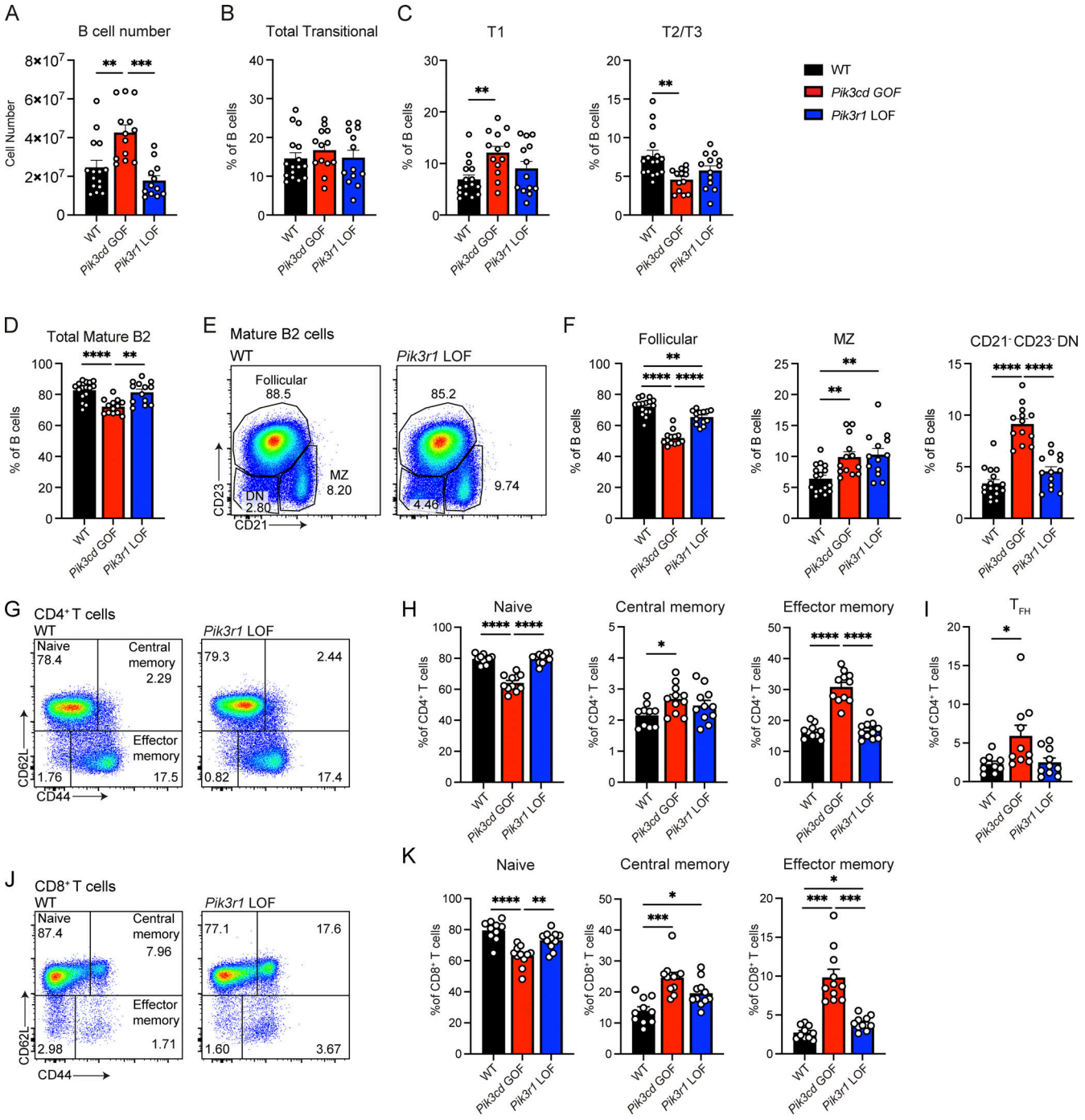

Figure 2. **Phenotype of lymphocytes in *Pik3r1* LOF mice.** Spleens from young (9–12 wk) WT, *Pik3cd* GOF, and *Pik3r1* LOF mice were stained to identify different lymphocyte populations by flow cytometric analysis. **(A)** Absolute number of B cells in the spleen. **(B)** Percentage of total transitional (B220$^+$ CD93$^+$) B cells. **(C)** Percentages of T1 (CD23$^-$) and T2/T3 (CD23$^+$) transitional B cells. **(D)** Percentage of mature (B220$^+$CD93$^-$) B cells. **(E and F)** Representative pseudocolor plots gated on WT or *Pik3r1* LOF mature B cells (E) with the percentages of mature B cell subsets, including follicular (CD21^{high}CD23^{high}), marignal zone (MZ; CD21^{high}CD23^{low}), and CD21$^-$ CD23$^-$ double-negative (DN) B cells shown in bar graphs (F). **(G and H)** Representative pseudocolor plots gated on WT or *Pik3r1* LOF CD4$^+$ T cells (G) with the percentages of naïve (CD62L^{hi}CD44^{lo}), central memory (CD62L^{hi}CD44^{hi}), and effector memory (CD62L^{lo}CD44^{hi}) CD4$^+$T cells show in in bar graphs (H). **(I)** Percentage of CD4$^+$Tfh population within CD4$^+$T cells. **(J and K)** Representative pseudocolor plots gated on WT or *Pik3r1* LOF CD8$^+$ T cells (J) with the percentages of naïve (CD62L^{hi}CD44^{lo}), central memory (CD62L^{hi}CD44^{hi}), and effector memory (CD62L^{lo}CD44^{hi}) CD8$^+$T cells show in bar graphs (K). All graphs show individual points for each mouse and mean ± SEM, *n* = 10–15 per group. Significant differences were determined by one-way ANOVA, *P < 0.05, **P < 0.01, ***P < 0.001, ****P < 0.0001.

compared to WT controls, similar to *Pik3cd* GOF mice (Fig. 2, E and F; Avery et al., 2018; Preite et al., 2018a; Stark et al., 2018; Wray-Dutra et al., 2018). However, *Pik3r1* LOF mice did not show an expanded population of $CD21^{-}CD23^{-}$ cells (Fig. 2, E and F).

The $CD4^{+}$ T cell compartment was largely unaffected by *Pik3r1* LOF, with normal percentages of naïve, memory, and Tfh cells in spleens of both young (Fig. 2, G–I) and aged (Fig. S2 J) mice irrespective of *Pik3r1* genotype. This was in marked contrast to *Pik3cd* GOF mice, which displayed increased Tfh cell and memory $CD4^{+}$ T cells. *Pik3r1* LOF mice also did not show significant dysregulation of the Treg compartment (Fig. S2, K and L). There were slight but significant increases in proportions of T_{CM} and T_{EM} populations in the $CD8^{+}$ T cell compartment of *Pik3r1* LOF mice, but this was much milder than the changes occurring in $CD8^{+}$ T cells due to the *Pik3cd* GOF allele (Fig. 2, J and K; and Fig. S2 M). Consistent with relatively intact peripheral T cell populations, we observed only minor changes in proportions of developing T cell populations in the thymus of *Pik3r1* LOF mice (Fig. S2 N). Thus, in the non-challenged state, *Pik3r1* LOF mice display far less dysregulation of their lymphocyte compartments than *Pik3cd* GOF mice.

Human *PIK3R1* LOF B cells show aberrant proliferation and differentiation in vitro

To assess how *PIK3R1* LOF mutations affected lymphocyte activation, we stimulated human naïve B cells in vitro and tracked proliferation using CFSE. Naïve B cells from *PIK3R1* LOF patients underwent greater proliferation than naïve B cells from healthy donors in response to a range of different stimuli (Fig. 3, A–D).

To confirm that this effect was due to increased PI3Kδ signaling, we determined whether the p110δ-specific inhibitor leniolisib (Hoegenauer et al., 2017; Rao et al., 2017) could normalize B cell proliferation. We found that 0.03 μM leniolisib effectively reduced proliferation of naïve B cells from healthy donors stimulated with CD40L/CpG (Fig. 3 E), with minimal effects on viability (data not shown). However, while 0.03 μM leniolisib effectively reduced the percentage of B cells from healthy donors that had entered division, it had only a mild effect on *PIK3R1* LOF B cells (Fig. 3 E). However, 0.3 μM leniolisib had a stronger effect, decreasing the proliferation of *PIK3R1* LOF B cells to similar levels as B cells from healthy donors in the absence of the inhibitor, both in terms of total divided cells and progression through division (Fig. 3, E and F). Thus, increased proliferation of *PIK3R1* LOF B cells resulted from excessive activity of PI3Kδ signaling, demonstrated by the normalization of this response by pharmacological inhibition of p110δ.

Hypogammaglobulinemia and reductions in frequencies of both total memory and IgG^{+} class-switched memory B cells in *PIK3R1* LOF patients could result from intrinsic B cell defects or be secondary to $CD4^{+}$ T cell defects. To establish intrinsic versus extrinsic defects in B cell class switching and plasma cell differentiation due to *PIK3R1* LOF mutations, transitional, naïve, and unswitched memory B cells were sort-purified and cultured with a variety of polyclonal stimuli; IgM, IgG, and IgA secretion was measured after 7 d. Strikingly, upon culture with CD40L and IL-21, a potent activator of B cell differentiation, class switching, and Ig secretion (Deenick et al., 2013; Recher et al., 2011), *PIK3R1* LOF transitional B cells secreted fourfold less IgM compared to transitional B cells from healthy donors (Fig. 3 G) and failed to produce detectable levels of the switched isotypes IgG and IgA (Fig. 3 G). In comparison, naïve and memory B cells from *PIK3R1* LOF patients generally had intact IgM secretion following stimulation with CD40L/IL-21 (Fig. 3, H and I) or CD40L/CpG and BCR engagement (Fig. 3 I). Unlike IgM production, *PIK3R1* LOF naïve B cells produced significantly reduced levels of IgG, and variable levels of IgA compared to naïve B cells from healthy donors (Fig. 3 H). *PIK3R1* LOF memory B cells from nearly all patients secreted significantly reduced levels of both IgG and IgA relative to memory B cells from healthy donors (Fig. 3 I), suggesting a severe switching defect.

Pik3r1 LOF also leads to dysregulated activation of murine B cells

We confirmed the impact of loss of regulatory PI3K function on B cell activation using cells from our mouse models. Consistent with our observations for human *PIK3R1* LOF B cells we also detected increased proliferation of *Pik3r1* LOF and *Pik3cd* GOF murine B cells compared to WT B cells under some conditions (Fig. S3 A). Further, *Pik3r1* LOF B cells showed severely blunted class switching to all Ig isotypes tested (IgG1, IgG2b, IgG3, IgE). This was comparable to impaired switching by *Pik3cd* GOF B cells (Fig. 4 A), except in cultures that contained TGFβ where the *Pik3r1* LOF B cells showed a more severe switching defect to IgG2b and IgG3 (Fig. 4 A). Class switching is linked to cell division (Deenick et al., 1999; Hodgkin et al., 1996). However, impaired Ig class switching by *Pik3r1* LOF or *Pik3cd* GOF B cells was not due to the altered proliferative capacity of these cells because switching was decreased across divisions for all culture conditions tested (Fig. 4 B). These data are consistent with the normal-to-increased levels of proliferation observed for human and murine *PIK3R1* LOF B cells (Fig. 3, A–D and Fig. S3 A). Altogether, these data show that *PIK3R1* LOF causes a significant defect in Ig class switching that is B cell intrinsic, and independent of cell division.

PIK3R1 LOF modulates cytokine production by human $CD4^{+}$ T cells

$CD4^{+}$ T cells from *PIK3CD* GOF patients or *Pik3cd* GOF mice have altered differentiation and cytokine production, most notably an increase in Th2 cytokines (Bier et al., 2019; Preite et al., 2019). To determine whether *PIK3R1* LOF also disturbed $CD4^{+}$ T cell function, we sorted memory $CD4^{+}$ T cells from patients and healthy donors, stimulated them with T cell activation and expansion (TAE, anti-CD2/CD3/CD28 mAb) beads for 5 d and compared expression and secretion of Th1 (IFNγ, TNFα), Th2 (IL-4, IL-5, IL-13), and Th17 (IL-17A. IL-17F, IL-22) cytokines, and IL-21 (Fig. 5, A–G). We observed significantly increased secretion of the Th2 cytokine IL-4, IL-5, and IL-13 (Fig. 5 D) as well as increased IL-22 (Fig. 5 F). Production of other cytokines by memory *PIK3R1* LOF $CD4^{+}$ T cells did not differ significantly from memory $CD4^{+}$ T cells from healthy donors (Fig. 5, A–G).

Pik3r1 LOF has cell intrinsic effect on cytokine production of murine $CD4^{+}$ T cells

Elucidating whether this effect of *PIK3R1* LOF on cytokine production by human memory $CD4^{+}$ T cells was intrinsic or extrinsic

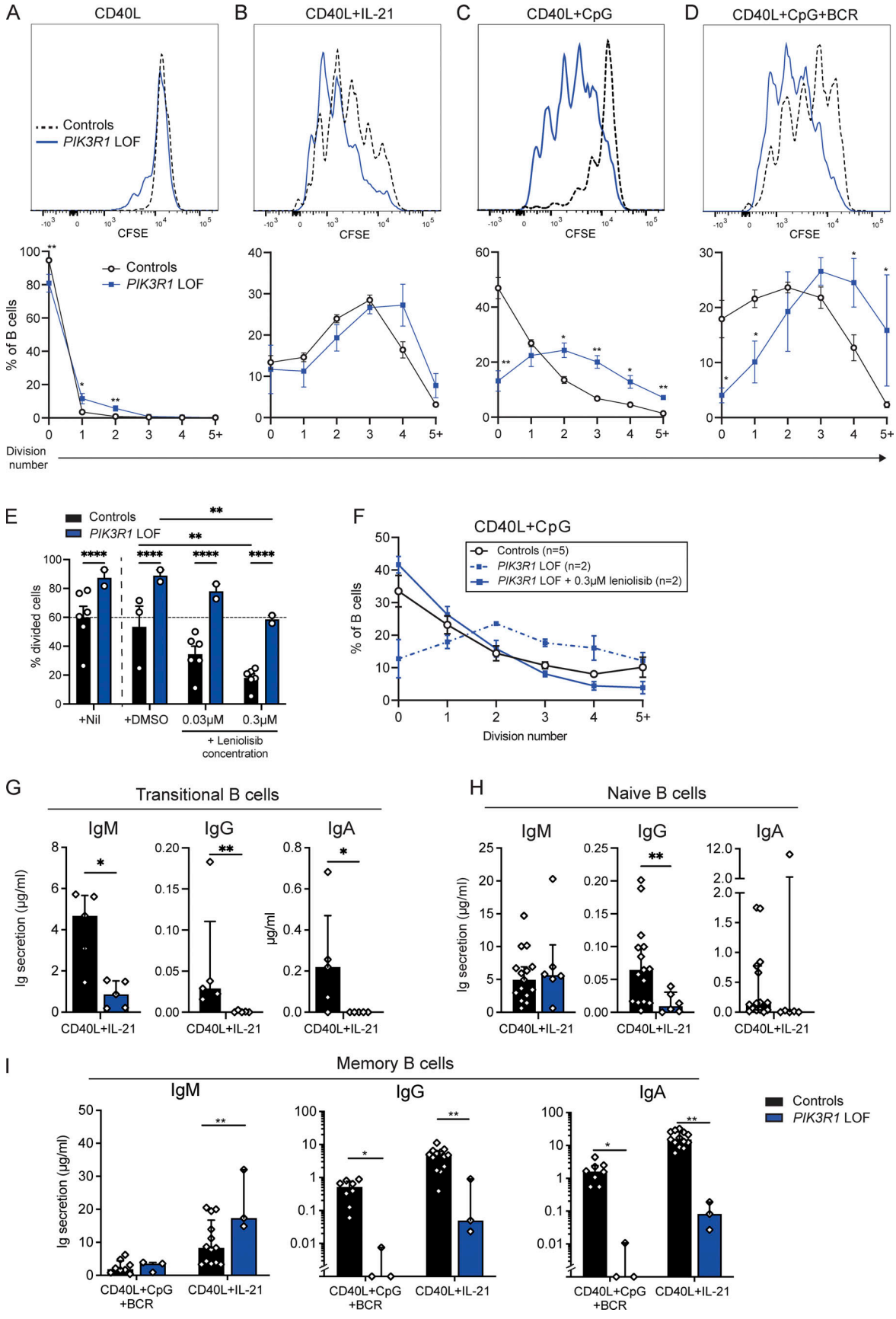

Figure 3. **Human *PIK3R1* LOF B cells have altered proliferation and Ig class switching in vitro. (A–D)** Naïve B cells from healthy donors (*n* = 13–18) and *PIK3R1* LOF patients (*n* = 2–3) were CFSE-labeled and cultured for 4 d with (A) CD40L alone or together with (B) IL-21, (C) CpG, or (D) CpG and SAC, a BCR

agonist. Cells were harvested after 4 d and labeled with Zombie Aqua, followed by flow cytometric analysis. Histograms overlay CFSE dilution of B cells from a healthy donor (black dotted line) and a *PIK3R1* LOF patient (blue line) from one representative experiment. Graphs below summarize CFSE dilution analysis for naïve B cells from healthy donors (n = 13–18) and *PIK3R1* LOF patients (n = 3), showing the frequency of cells in each division interval. Data combined from three independent experiments. **(E and F)** Naïve ($CD27^-CD10^-$) or $CD27^-$ B cells from healthy donors (n = 3–6) and *PIK3R1* LOF patients (n = 2) were cultured with CD40L and CpG in the absence or presence of two different concentrations of leniolisib. DMSO was added as a control. CFSE dilution analysis of control and *PIK3R1* LOF B cells treated with 0.3 µM leniolisib shown as frequency of cells in each division interval. Each point represents a different individual, data combined from two independent experiments, bars represent mean ± SEM. Statistical significance was determined by Mann–Whitney tests, **P < 0.01, ****P < 0.0001. **(G–I)** Sort-purified (G) transitional, (H) naïve, and (I) unswitched memory B cells from healthy donors (n = 5–15) and *PIK3R1* LOF patients (n = 3–6) were cultured with CD40L together with IL-21, or CpG and SAC. After 7 d, the amount of IgM, IgG, and IgA secreted into the culture supernatant was measured by ELISA. Each point represents a different individual, results combined from at least three independent experiments, bars show median and interquartile ranges. Statistical significance was determined by Mann–Whitney tests, *P < 0.05, **P < 0.01.

was complicated by at least two experimental challenges. First, the small number of naïve $CD4^+$ T cells in *PIK3R1* LOF patients precluded a detailed analysis of the impact of an intrinsic increase in PI3K signaling on their capacity to differentiate into different Th subsets. Second, altered cytokine production from memory $CD4^+$ T cells could result from extrinsic factors such as infection, interactions with other cells or treatments the patients may be receiving. To overcome these limitations, we used our mouse model of *Pik3r1* LOF to assess naïve $CD4^+$ T cell differentiation in response to different Th polarizing conditions. Compared to WT $CD4^+$ T cells, fewer *Pik3r1* LOF and *Pik3cd* GOF $CD4^+$ T cells were recovered from Th0 and Th1 cultures, suggesting decreased cell survival and/or proliferation in vitro (Fig. 6 A). However, when we measured intracellular cytokine expression by the surviving cells, we found that increased PI3K signaling due to either *Pik3r1* LOF or *Pik3cd* GOF led to significant increases in proportions of cells expressing IFNγ and IL-5 over WT $CD4^+$ T cells, as well as a trend toward decreased IL-17A expression (Fig. 6, B–D). Production of TNFα was unaffected by *Pik3r1* LOF (Fig. S3 B). Thus, altered PI3K signaling skews both human and mouse $CD4^+$ T cell differentiation, most notably leading to increased Th2 responses consistent with the Th2-related pathologies seen in APDS patients (Bier et al., 2019; Maccari et al., 2018).

Impact of *Pik3r1* LOF on murine B cell responses in vivo

In vitro analyses established that *PIK3R1* LOF intrinsically compromises B cell function. However, the generation of a robust, durable, and effective B cell antibody (Ab) response involves the coordinated interactions of numerous cells, a scenario that cannot be fully replicated in vitro. Thus, to elucidate mechanisms underlying defective Ab responses in patients with *PIK3R1* LOF mutations, we used our *Pik3r1* LOF mouse model to track the kinetics and magnitude of a T-dependent B cell response in vivo. *Pik3r1* LOF mice were crossed with SW_{HEL} mice, which express a BCR specific for hen-egg lysozyme (HEL; Phan et al., 2003). WT or *Pik3r1* LOF SW_{HEL} cells were transferred to WT recipient mice which were then immunized with a low-affinity variant of HEL (HEL-2x; Paus et al., 2006) conjugated to sheep red blood cells (SRBC). In this scenario, only the transferred responding B cells are *Pik3r1* LOF, while all other cells are WT, thereby enabling the B cell–intrinsic effects of *Pik3r1* LOF to be determined. After immunization with HEL-2x, both WT and *Pik3r1* LOF SW_{HEL} B cells rapidly expanded, peaking around day 5.5 and then contracting. While *Pik3r1* LOF and WT SW_{HEL} cells showed a similar pattern of expansion and contraction, the magnitude of the response by *Pik3r1* LOF SW_{HEL} B cells was significantly lower than WT SW_{HEL} B cells (Fig. 7 A). Despite this decreased expansion, the percentage of *Pik3r1* LOF SW_{HEL} B cells that became short-lived plasmablasts or germinal center (GC) B cells was similar to WT SW_{HEL} cells (Fig. 7 B). However, consistent with the in vitro analyses, both plasmablasts and GC B cells generated from *Pik3r1* LOF SW_{HEL} B cells displayed significantly decreased class switching, evidenced by increased IgM^+ and fewer $IgG1^+$ cells—usually the largest portion of responding cells—compared to plasmablasts and GC B cells generated from WT SW_{HEL} B cells (Fig. 7, C and D). This alteration in Ig isotype was also observed at the level of serum anti-HEL Ab, with significant increases and decreases in HEL-specific IgM and IgG1, respectively, in mice receiving *Pik3r1* LOF B cells compared to WT B cells (Fig. 7 E).

Pik3r1 LOF impairs affinity maturation of evolving murine B cell responses in vivo

Class switching and somatic hypermutation (SHM) are linked mechanistically, as both require cell division and activation-induced cytidine deaminase. To analyze affinity maturation during the in vivo B cell response, we examined SHM within the Ig heavy chain variable gene expressed by *Pik3r1* LOF and WT SW_{HEL} GC B cells on day 10. The average number of mutations per sequence was similar in WT and *Pik3r1* LOF SW_{HEL} B cells (2.22 ± 0.16 vs. 2.02 ± 0.28 for IgM^+ cells, n = 4 mice, 97 cells total [WT] and n = 5 mice, 76 cells [*Pik3r1* LOF], 2.28 ± 0.13 vs. 2.28 ± 0.26 for $IgG1^+$ cells, n = 4 mice 108 cells total [WT] and n = 5 mice, 55 cells total [*Pik3r1* LOF]). Thus, unlike class switching, SHM per se was not affected by *Pik3r1* LOF.

However, when we focused on the canonical Y53D mutation—which underpins affinity maturation in the SW_{HEL} system (Phan et al., 2006)—we observed ∼2-fold fewer *Pik3r1* LOF SW_{HEL} cells that expressed the Y53D mutation compared to WT SW_{HEL} cells, irrespective of Ig isotype (Fig. 7 F). Affinity maturation is an iterative process that requires cycling between the dark zone (DZ) and the light zone (LZ) of the GC (Brink and Phan, 2018). Thus, we assessed whether the distribution of GC B cells within the LZ and DZ compartments was altered by *Pik3r1* LOF. This revealed that the ratio of DZ to LZ cells was decreased in *Pik3r1* LOF GCs compared to WT GCs (Fig. 7 G). Thus, *Pik3r1* LOF not only compromises proliferation and class switching by Ag-specific B cells in vivo, but also impairs affinity maturation.

Pik3r1 LOF $CD4^+$ T cells provide poor help to B cells

While these results indicate that *Pik3r1* LOF mutations cause a significant impairment in the ability of B cells to generate an

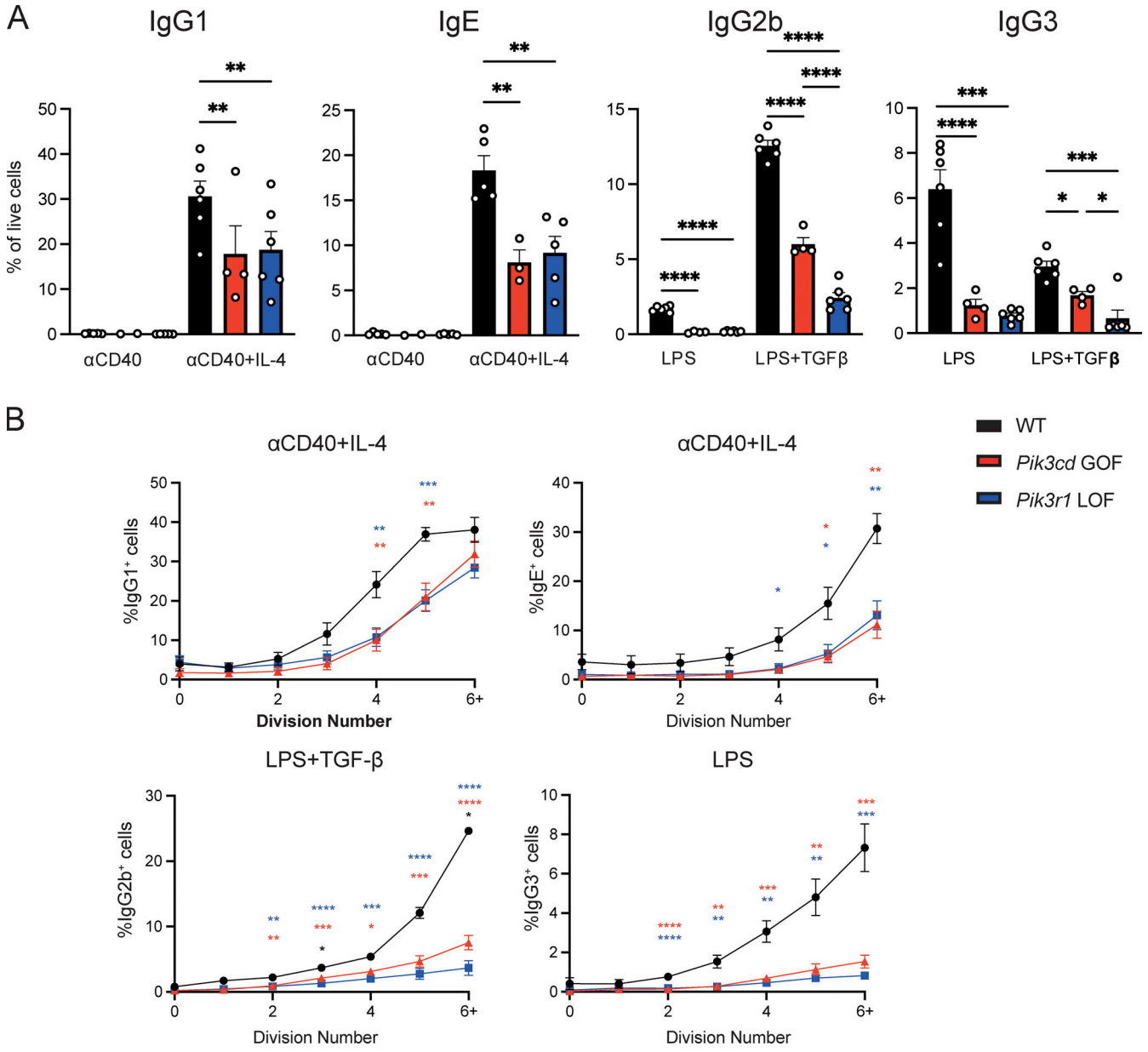

Figure 4. **Murine *Pik3r1* LOF B cells have reduced switching.** Follicular B cells (B220⁺CD93⁻CD21^{high}CD23^{high}) were sorted from spleens of young (9–12 wk) WT, *Pik3cd* GOF, and *Pik3r1* LOF mice. Cells were labeled with CellTrace Yellow and stimulated with αCD40 alone, αCD40+IL-4, LPS alone, or LPS + TGFβ for 4 d. Cells were then harvested and stained for IgG1, IgE, IgG2b, and IgG3 as shown. **(A)** Graphs show total percentage of switched cells of each isotype. Each point represents a separate experiment, bars give mean ± SEM, *n* = 2–5 as shown. **(B)** Graphs show percentage of switched cells per division. All graphs show mean ± SEM from 4–8 independent experiments. Significant differences between WT and *Pik3cd* GOF, WT and *Pik3r1* LOF, and *Pik3cd* GOF and *Pik3r1* LOF B cells are indicated in red, blue, and black, respectively. Significant differences were determined by one-way ANOVA, *P < 0.05, **P < 0.01, ***P < 0.001, ****P < 0.0001.

effective Ab response, protective Ab responses are also dependent on Tfh cells (Deenick and Ma, 2011; Tangye et al., 2013). Thus, we determined whether *Pik3r1* LOF mutation also affected Tfh cell differentiation and function. *Pik3r1* LOF mice were crossed with OT-II mice (Barnden et al., 1998), which express a transgenic TCR recognizing an OVA peptide. OT-II cells were then adoptively transferred into signaling lymphocytic activation molecule-associated protein (SAP/*Sh2d1a*$^{-/-}$)-deficient hosts and immunized with OVA. Endogenous SAP-deficient CD4⁺ T cells are unable to provide effective help to B cells (Crotty et al., 2003). Thus, any B cell response generated is a direct measure of the help provided by transferred WT or *Pik3r1* LOF OT-II cells.

7 d after OVA immunization, expansion of WT and *Pik3r1* LOF OT-II cells was similar (Fig. 8 A). The percentage of OT-II cells that acquired a Tfh phenotype (Fig. 8 B) was also comparable for WT and *Pik3r1* LOF cells indicating that increased PI3K signaling did not significantly alter differentiation of naïve CD4⁺ T cells to Tfh cells. Strikingly, despite comparable frequencies of Tfh cells, the number of GC B cells arising from WT B cells was significantly reduced in mice that received *Pik3r1* LOF OT-II cells compared to those receiving WT OT-II cells (Fig. 8 C). We also

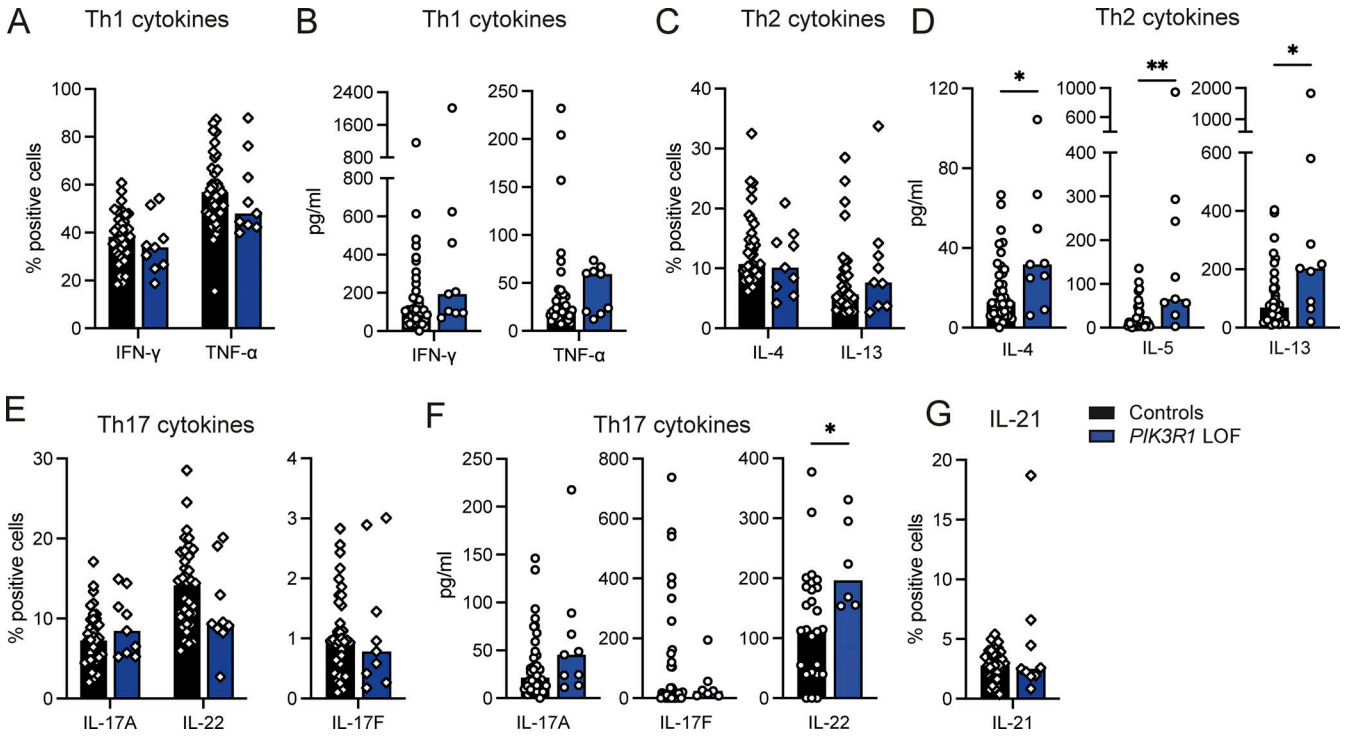

Figure 5. **Human *PIK3R1* LOF CD4⁺ T cells have altered cytokine production. (A–G)** Sort-purified memory CD4⁺ T cells from healthy controls (n = 26–37) and *PIK3R1* LOF patients (n = 6–9) were cultured for 5 d with TAE beads. (A, C, E, and G) Intracellular expression and (B, D, and F) secretion of (A and B) Th1, (C and D) Th2, or (E and F) Th17 cytokines were determined by intracellular staining and cytometric bead arrays, respectively. **(G)** IL-21 expression was determined by intracellular staining. Each point represents a different individual, bars show median, data combined from nine independent culture experiments. Statistical significance was determined using Mann–Whitney tests, *P < 0.05, **P < 0.01.

assessed the levels of OVA-specific Abs that were secreted into the serum, which revealed a significant decrease in anti-OVA IgM from B cells that received help from *Pik3r1* LOF CD4⁺ T cells (Fig. S3 C). Thus, *Pik3r1* LOF CD4⁺ T cells are less capable of providing help to WT B cells to generate Ab-secreting cells and seed GC responses than WT CD4⁺ T cells. Furthermore, *Pik3r1* LOF OT-II T cells displayed altered cytokine production with decreased IL-2 (Fig. 8 D), but no significant differences in IFNγ or IL-17 (Fig. 8, E and F). However, despite reduced GC B cells and altered CD4⁺ T cell cytokine profiles, class switching by GC B cells was not altered (Fig. S3, D–F).

Differences in the effects of *Pik3r1* LOF and *Pik3cd* GOF mutations on downstream signaling

Our studies revealed many similarities between the cellular alterations caused by *Pik3r1* LOF and *Pik3cd* GOF mutations, but

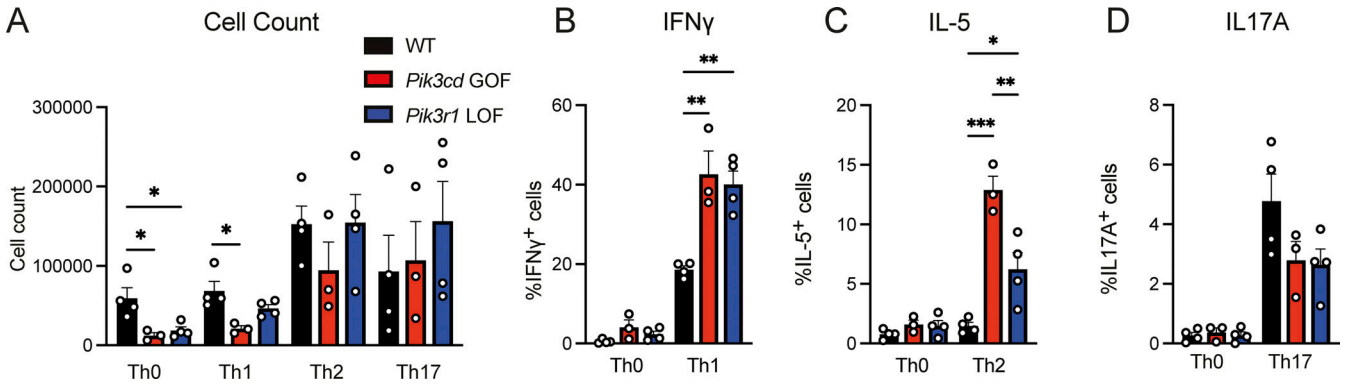

Figure 6. **Mouse *Pik3r1* CD4⁺ T cells also show dysregulated cytokine production.** Naïve CD4⁺ T cells (CD4⁺CD44^{lo}CD62L^{hi}) were sorted from spleens of WT, *Pik3cd* GOF, or *Pik3r1* LOF mice, stimulated with anti-CD3 and anti-CD28 mAbs under polarizing conditions for 4 d and then restimulated with PMA/ionomycin. **(A)** Average count of live cells in each culture condition. **(B–D)** Cells were harvested and stained for intracellular expression of (B) IFNγ, (C) IL-5, and (D) IL17A. Graphs depict cytokine production under each condition as stated under each graph. Significant differences were determined by one-way ANOVA, *P < 0.05, **P < 0.01, ***P < 0.001. Each point represents a separate mouse, bars show mean ± SEM from four independent experiments.

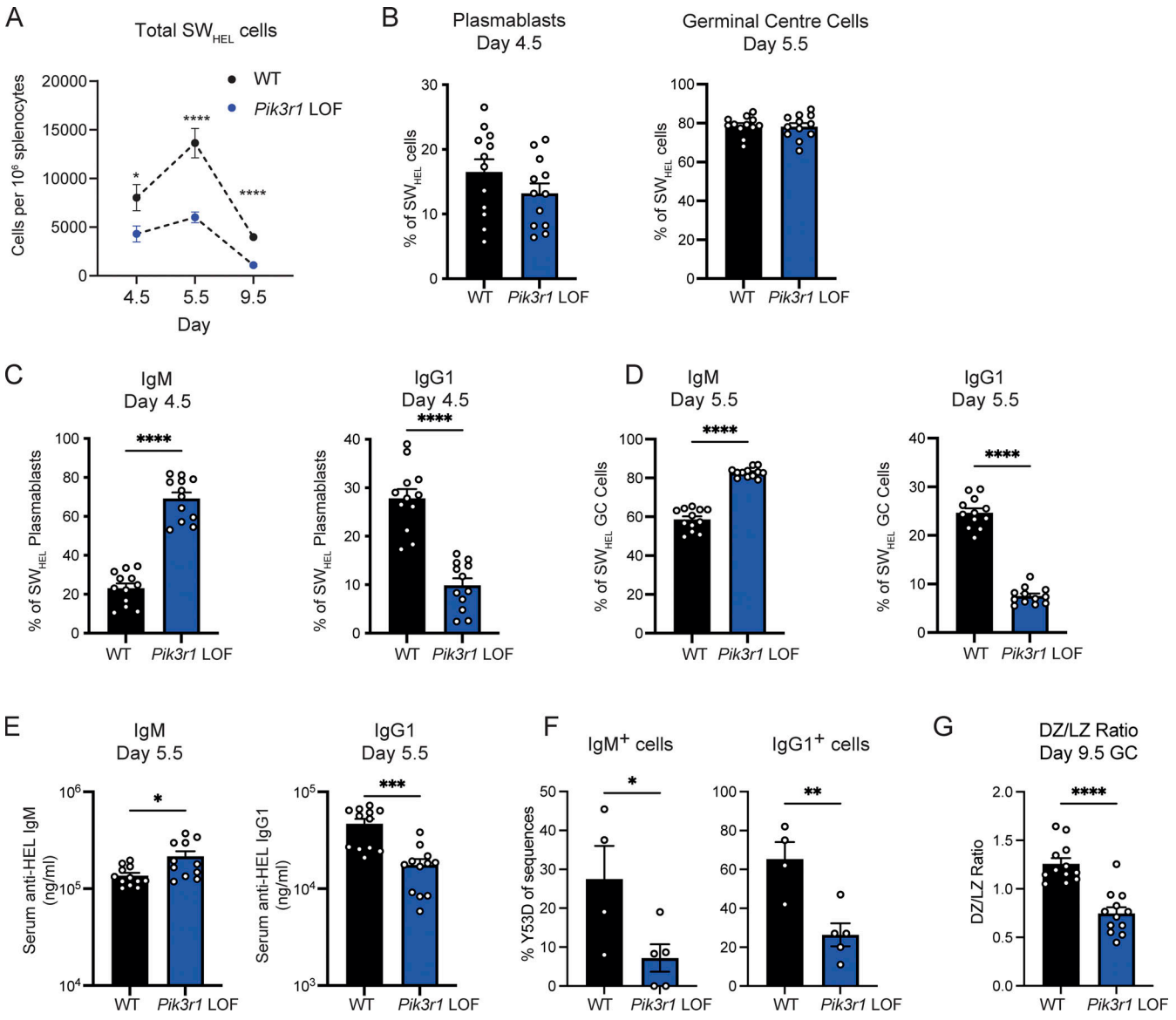

Figure 7. ***Pik3r1* LOF B cells show impaired expansion, switching, and affinity maturation in vivo.** WT or *Pik3r1* LOF SW$_{HEL}$ cells were transferred to WT congenic hosts, which were then immunized with HEL-2x-SRBC. **(A)** The expansion of SW$_{HEL}$ cells was tracked over time. **(B)** Percentage of cells with a plasmablast (CD138$^+$) or GC (CD38^{lo}Fas^{hi}) phenotype was determined. **(C and D)** Percentage of cells that were unswitched (IgM$^+$) or switched to IgG1 were determined in the (C) plasmablast and (D) GC populations. **(E)** Levels of HEL-specific serum IgM and IgG1 at day 5.5 were determined by ELISA. **(F)** Donor GC IgM or IgG1$^+$ cells were sorted on day 9.5 and sequenced to identify mutations. **(G)** The ratio of DZ to LZ cells in the GC was determined by CXCR4 and CD86 staining. Each point represents one mouse, bars show mean ± SEM, *n* = 12 from three experiments, except F, *n* = 4–5 from two experiments. Significant differences were determined by Mann–Whitney, *P < 0.05, **P < 0.01, ***P < 0.001, ****P < 0.0001.

also several striking differences (Table 1). There are several potential explanations for these differences. First, while it is clear that both *Pik3cd* GOF and *Pik3r1* LOF can increase PI3K signaling, the magnitude and nature of this increase may be different. Second, as p85α interacts not only with p110δ but also the other p110 catalytic subunits, this may lead to overactivation of these subunits as well. To explore differences between *Pik3r1* LOF and *Pik3cd* GOF further we examined signaling downstream of PI3K. Follicular B cells were sorted from WT, *Pik3r1* LOF and *Pik3cd* GOF mice and stimulated with anti-IgM or anti-CD40 Ab and p-S6 tracked over time by flow cytometry. *Pik3cd* GOF displayed increased p-S6 compared to WT in response to both anti-Ig and anti-CD40 (Fig. 9, A and B). In contrast, p-S6 in *Pik3r1* LOF B cells was significantly lower than in *Pik3cd* GOF B cells in response to anti-IgM but not in response to anti-CD40. This suggested that *Pik3cd* GOF and *Pik3r1* LOF alter signaling downstream of PI3K in different ways and that this is also dependent on the type of stimulation the cell receives. We investigated this further by examining phosphorylation of other molecules involved in PI3K signaling. Sorted follicular B cells were left unstimulated or stimulated for 30 min with anti-Ig or anti-CD40 and phosphorylation of different substrates measured using a multiplexed assay. This revealed significantly more elevated activation of Akt in *Pik3cd* GOF B cells, irrespective of

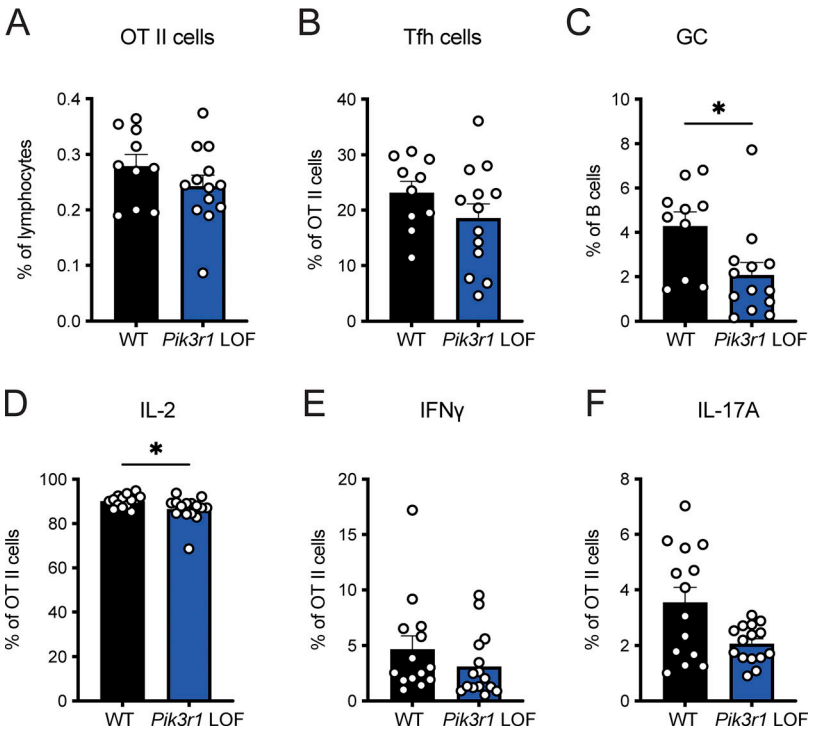

Figure 8. ***Pik3r1* LOF Tfh cells have impaired ability to provide help to B cells.** WT or *Pik3r1* LOF OT-II T cells were transferred into SAP^{KO} recipients, which were then immunized with OVA/Alum intraperitoneally. Spleens were harvested 7 d later and flow cytometry analysis was performed. **(A)** Percentages of OT-II cells recovered 7 d after transfer. **(B)** Percentage of Tfh ($CXCR5^+PD\text{-}1^+$) cells in the OT-II population. **(C)** Percentage of GC B cells ($B220^+Fas^{hi}CD38^{lo}$) in recipient mice. **(D–F)** Recipient splenocytes harvested at day 7 were stimulated ex vivo with PMA/ionomycin for 6 h and intracellular cytokine staining was performed to identify OT-II cells expressing (D) IL-2, (E) IFNγ, and (F) IL-17A. Each point represents a different mouse, combined data from three independent experiments, bars show Mean ± SEM, n = 10–13. Significant differences were determined by Mann–Whitney, *P < 0.05.

stimulation (Fig. 9, C–E). In contrast, Akt phosphorylation was only significantly upregulated in *Pik3r1* LOF B cells compared to WT B cells in response to anti-CD40 Ab (Fig. 9, C–E). We observed similar patterns for pGSK3β and pTSC2 which are phosphorylated by Akt (Bilanges et al., 2019; Fig. S4, A–C). Interestingly we also saw strikingly increased phosphorylation of

Table 1. **Features of APDS1 and APDS2**

	***PIK3R1* LOF patients**	***Pik3r1* LOF mice**	***PIK3CD* GOF patients**	***Pik3cd* GOF mice**
Bone marrow	• ↓ Mature B cells • **↑ Pro-B cells**	• Normal mature cells • **↑ Pro-B cells**	• ↓ Mature B cells • **↑ Pre-B cells**	• ↓ Mature B cells • **↑ Pre-B cells**
Peripheral B cells	• ↑ Transitional cells • ↓ Naïve and memory •**↓ IgG^+ memory B cells**	• **Normal total B cells** • ↑ Marginal zone cells •↓ Follicular cells	• ↑ Transitional cells • ↓ Naïve and memory •**↓ IgG^+, IgA^+ memory B cells**	• **↑ Total B cells** • ↑ Marginal zone cells •↓ Follicular cells
B cell activation	• ↑ Proliferation in vitro • ↓ Ig class switching	• ↑ Proliferation in vitro • ↓ Ig class switching	• ↑ Proliferation in vitro • ↓ Ig class switching	• ↑ Proliferation in vitro • ↓ Ig class switching
B cell response to immunization		• **↓ Expansion** • Normal GC and plasmablast differentiation •↓ Ig class switching •Normal SHM •**↓ Affinity maturation**		• **Normal expansion** • Normal GC and plasmablast differentiation •↓ Ig class switching •Normal SHM •**Normal affinity maturation**
T cells	• ↓ Naïve and ↑ memory $CD4^+$ and $CD8^+$ T cells	• **Normal naïve $CD4^+$ and $CD8^+$ T cells**, ↑ $CD8^+$ effector memory cells	• ↓ Naïve and ↑ memory $CD4^+$ and $CD8^+$ T cells in patients	• **↓ Naïve and $CD4^+$ and $CD8^+$ T cells**, ↑memory T cells in mice (cell extrinsic effect)
T cell differentiation	• ↑ Th2 cells • **Normal % Tfh ex vivo**	• ↑ Th2 cells • **Normal % Tfh preimmunization** •**Normal $CD4^+$ T cell expansion to immunization** •↓ Tfh function	• ↑ Th2 cells • **↑ % Tfh ex vivo**	• ↑ Th2 cells • **↑ % Tfh preimmunization** •**↓ $CD4^+$ T cell expansion to immunization** •↓ Tfh function
Extra immune phenotype		• **↓ Mutant pups at weaning** • **↓Weight**		• **Normal Mendelian ratios**

Differences between APDS1 and APDS2 are indicated in bold.

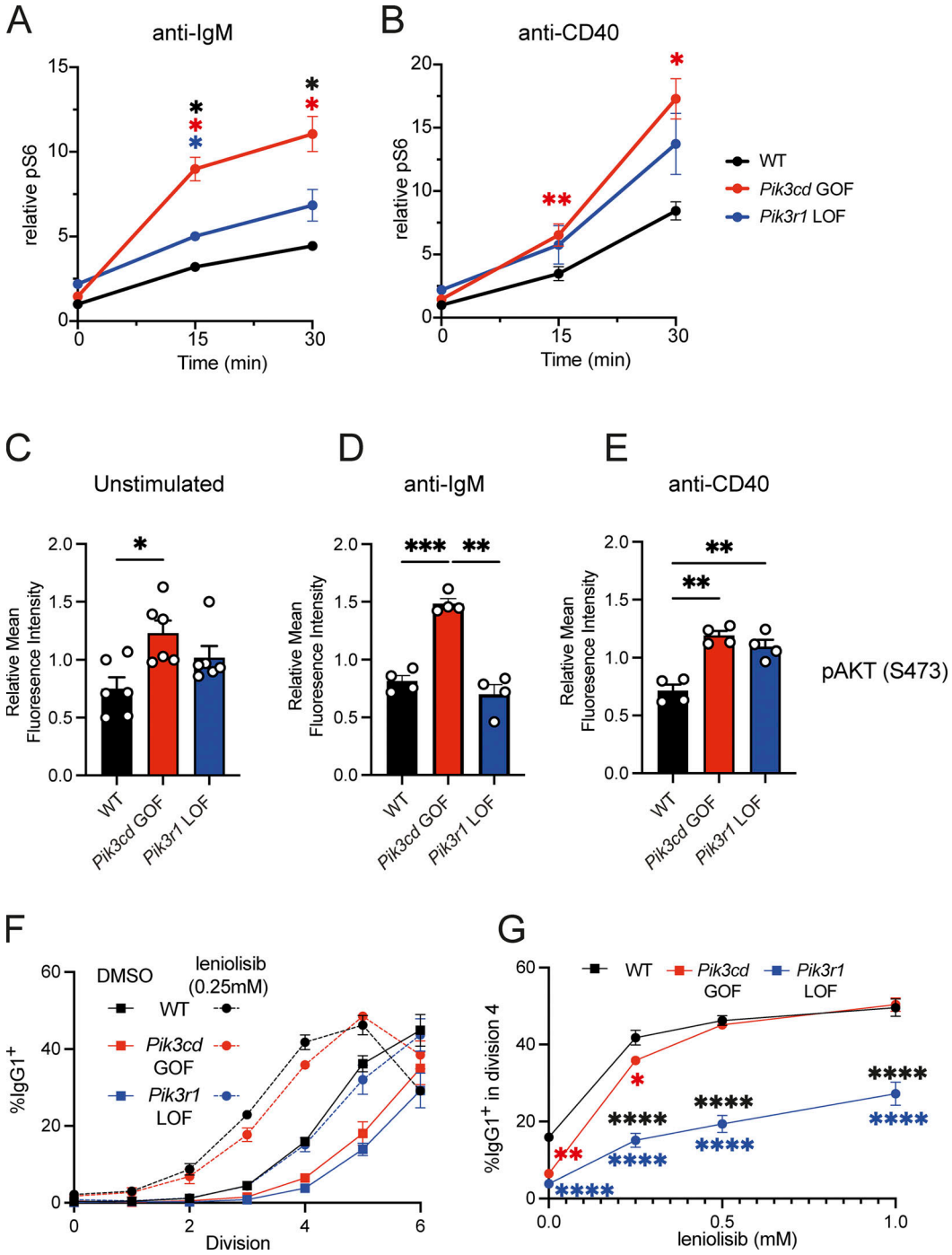

Figure 9. ***Pik3r1* LOF and *Pik3cd* GOF murine B cells show different alterations in signaling.** Follicular B cells (B220⁺CD93⁻CD21^{high}CD23^{high}) were sorted from spleens of WT, *Pik3cd* GOF, and *Pik3r1* LOF mice. **(A and B)** Cells were stimulated with (A) αIgM or (B) αCD40, and p-S6 was detected by flow cytometry at the indicated times. Plots show mean ± SEM, *n* = 4. Significant differences between WT and *Pik3cd* GOF, WT and *Pik3r1* LOF, and *Pik3cd* GOF and *Pik3r1* LOF B cells are indicated in red, blue, and black, respectively. Significant differences were determined by one-way ANOVA; *P < 0.05, **P < 0.01. **(C–E)** Cells were left unstimulated (C) or stimulated with αIg (D) or αCD40 (E) for 30 min. Total cell lysates were prepared and pAkt (S473) was determined using the Milliplex MAP Total Akt/mTOR Magnetic Bead 11-Plex Kit. Values were normalized to mean values for each experiment. Each point represents an individual sorted B cell population from different mice, from at least three independent experiments, bars give mean ± SEM, *n* = 4–6. Significant differences were calculated by one-way ANOVA; *P < 0.05, **P < 0.01, ***P < 0.001. **(F and G)** Cells were labeled with CellTrace Yellow and stimulated with αCD40+IL-4 for 4 d in the presence of DMSO (control) or various concentration of leniolisib as shown. Cells were then harvested and stained for IgG1. **(F)** Graphs show percentage of switched cells per division. **(G)** The percentage of IgG1⁺ switched cells in division 4 was plotted for each concentration of inhibitor. **(F and G)** Graphs show mean ± SEM from three independent experiments. Significant differences were calculated by two-way ANOVA *P < 0.05, **P < 0.01, ****P < 0.0001.

phosphatase and tensin homolog (PTEN) at Ser 380, a site which has been reported to lead to decreased PTEN phosphatase activity (Vazquez et al., 2000).

To determine whether other p110 catalytic subunits may be playing a role, we determined whether the changes we observed in *Pik3r1* LOF cells were dependent on PI3Kδ. Follicular B cells were stimulated with anti-CD40 Ab and IL-4 and the p110δ inhibitor leniolisib was added at concentrations previously shown to restore switching in *Pik3cd* GOF B cells (Avery et al., 2018). While high doses of leniolisib were able to increase the levels of switching in *Pik3r1* LOF B cells, this did not reach the same levels seen in WT or *Pik3cd* GOF B cells treated with high doses (Fig. 9, F and G). Indeed, the dose response curve suggested that switching in *Pik3r1* LOF cells plateaued at approximately half the level of that seen in WT or *Pik3cd* GOF cells (Fig. 9 G). An even more striking failure to restore switching was observed for switching to IgE (Fig. S4 D).

Discussion

APDS1 (caused by *PIK3CD* GOF mutations) and APDS2 (caused by *PIK3R1* LOF mutations) have largely been considered to be clinical, cellular, and mechanistic phenocopies of each other. However, while we and others have extensively reported molecular and cellular immune defects due to *PIK3CD* GOF (Al Qureshah et al., 2021; Angulo et al., 2013; Avery et al., 2018; Bier et al., 2019; Cannons et al., 2018; Edwards et al., 2019; Jia et al., 2021; Lau et al., 2020; Lucas et al., 2014a; Preite et al., 2018a; Preite et al., 2018b; Stark et al., 2018; Wentink et al., 2018; Wray-Dutra et al., 2018), detailed analysis of the effects of *PIK3R1* LOF on immune function has not previously been undertaken. Our comprehensive analyses of humans and mice have revealed multiple effects of *PIK3R1* LOF on both T and B cells, thereby explaining some of the clinical features of APDS2 patients. Interestingly, while we observed significant overlap in cellular defects in APDS1 and APDS2, we also identified some important differences (Table 1) that highlight the complexities of PI3K-mediated regulation of cellular processes and function.

Both *PIK3R1* LOF or *PIK3CD* GOF mutations affected B cell development, albeit at different stages, impeding development at the pro-B and pre-B stages, respectively. Further, both *PIK3R1* LOF and *PIK3CD* GOF human and murine B cells exhibited significantly decreased Ig class switching. However, despite these aspects of B cell development and differentiation being impaired in vivo and in vitro, *Pik3r1* LOF and *Pik3cd* GOF B cells displayed intact generation of plasmablasts and GC B cells and normal overall rates of SHM following immunization with model T cell dependent antigens.

Strikingly, *Pik3r1* LOF, but not *Pik3cd* GOF, B cells showed significantly decreased expansion in vivo. This contrasts with the increased proliferation we observed in vitro and may reflect altered signals or competition in vivo that compromise survival of *Pik3r1* LOF B cells. Further, while the overall rate of SHM per se was unaffected, *Pik3r1* LOF, but not *Pik3cd* GOF, B cells showed poor affinity maturation following immunization. This suggests that while loss of the *PIK3R1* encoded regulatory subunit of PI3K does not impede the actual process of SHM, it prevents effective selection of high-affinity clones. Interestingly, this pattern of normal SHM but decreased affinity maturation has been seen in a number of other studies including in B cells lacking STAT3 or FOXO1, or in B cells with overactive p110α (Dominguez-Sola et al., 2015; Kane et al., 2016; Sander et al., 2015). Affinity maturation involves iterative rounds of selection of high-affinity cells in the LZ of the GC, followed by further expansion in the DZ (Brink and Phan, 2018). Thus, disruption of the LZ/DZ or decreased expansion of high-affinity B cells in the DZ can lead to poor affinity maturation. Indeed, it has been demonstrated that FOXO1 deficiency leads to a loss of the GC DZ (Dominguez-Sola et al., 2015; Sander et al., 2015). As PI3K inhibits FOXO1 activity, expression of an active p110α or deletion of PTEN, which negatively regulates PI3K activity, also leads to a decrease in the GC DZ. Thus, it is likely that increased PI3K activity due to *Pik3r1* LOF also dysregulates affinity maturation by disrupting the GC DZ. Consistent with this, we observed a decreased ratio of DZ to LZ cells in GCs in mice 10 d after receiving transferred *Pik3r1* LOF B cells.

In the T cell compartment, patients with either *PIK3R1* LOF or *PIK3CD* GOF mutations had decreased proportions of naïve T cells and increased memory cells. However, while these changes in T cell populations were replicated fully in *Pik3cd* GOF mice, they were not observed in *Pik3r1* LOF mice. We previously showed that in *Pik3cd* GOF mice these changes are not cell intrinsic (Bier et al., 2019) but rather are driven by other, hitherto unidentified extrinsic factors. The reduced aberrant T cell activation in *Pik3r1* LOF mice compared to *Pik3cd* GOF mice suggests that these extrinsic factors are limiting in *Pik3r1* LOF mice. However, in the patients it would be envisaged that other factors such as chronic infections may drive activation and expansion of memory T cell populations. Nevertheless, *Pik3r1* LOF did lead to significant cell-intrinsic functional changes in $CD4^+$ T cells with decreased ability of Tfh cells to support a GC reaction comprising WT B cells, and increased Th2 responses. The decreased Tfh functionality of *Pik3r1* LOF $CD4^+$ T cells likely exacerbates the B cell intrinsic defects in Ab production, thereby combining to cause the severely blunted protective Ab responses that are characteristic of APDS2 patients.

The mechanisms underlying these differences between the effects of *PIK3R1* LOF and *PIK3CD* GOF on lymphocytes are unknown. While it is clear that the mutant p85α subunit encoded by *PIK3R1* LOF mutations can increase signaling activity of the p110δ catalytic subunit, the magnitude and dynamics of this increase are likely to vary. Indeed, analysis of the kinase activity of p110δ in complex with mutant p85α showed an ∼200-fold increase in basal activity compared to the WT p85α/p110δ complex (Dornan et al., 2017). In contrast, the recurrent E1021K GOF mutation in p110δ itself only resulted in an ∼20-fold increase in activity (Dornan et al., 2017). Conversely, following activation, the E1021K GOF p110δ mutation caused a slightly higher increase in kinase activity than did the p85α mutant (Dornan et al., 2017). This is consistent with our results, where in unstimulated cells the increase in PI3K activity, as measured by pS6, was higher in *Pik3r1* LOF B cells than in *Pik3cd* GOF B cells (Fig. S2 F). However, on stimulation, particularly in response to anti-IgM, *Pik3cd* GOF led to much greater activation of

downstream signaling pathways. In contrast, this difference was less apparent in response to anti-CD40. Thus, while it is not clear what threshold of increased signaling needs to be achieved to alter cellular behavior at each stage of lymphocyte development and differentiation, it is likely that as cells encounter distinct stimuli these two mutations will result in different degrees of altered signaling which will dynamically impact cells at different stages. For example, it could be envisaged that increased signaling downstream of the BCR may drive the increased changes in B cell phenotype observed in *Pik3cd* GOF mice, while the altered CD40 signaling would be important for the T-dependent Ab responses which affects both *Pik3cd* GOF and *Pik3r1* LOF B cells. Another explanation for the differences between the phenotype of *PIK3R1* LOF and *PIK3CD* GOF cells is the ability of the *PIK3R1* encoded regulatory subunits such as p85α to interact with the p110α and p110β catalytic subunits, in addition to p110δ. It has been reported that mutant p85α does not cause the same level of hyperactivation of p110α as it does of p110δ, particularly in the basal state, however some level of hyperactivation is observed (Dornan et al., 2017). Here, our data suggests that the *Pik3r1* LOF may intrinsically suppress B cell Ig class switching by a p110δ independent pathway, suggesting that the activity of other p110 subunits, most likely p110α, is also increased. Thus, activation of other p110 catalytic subunits will also alter the cellular impacts and may underlie the differences between APDS1 and APDS2.

Interestingly, we found that at weaning, the numbers of *Pik3r1* LOF pups deviated dramatically from the expected Mendelian ratios, being ∼50% lower than predicted. This suggests that 50% of *Pik3r1* LOF pups were dying at the fetal stage or soon after birth. This pattern was not observed in *Pik3cd* GOF mice. This difference probably reflects both the wider expression of *Pik3r1* versus *Pik3cd* in non-immune/non-hematopoietic tissues and interactions between *Pik3r1*-encoded regulatory subunits with p110α and p110β, which similarly show broader expression than p110δ (Chantry et al., 1997; Okkenhaug, 2013). Consistent with an important role for *Pik3r1* expression outside the immune system, mice that completely lack p85α, p55α, and p50α regulatory subunits have high rates of perinatal lethality, and develop hypoglycemia and liver necrosis (Fruman et al., 2000). Further, patients with *PIK3R1* LOF mutations have higher rates of failure to thrive and neurological features than *PIK3CD* GOF patients (Elkaim et al., 2016; Jamee et al., 2019; Maccari et al., 2018). However, our analysis revealed no alterations in insulin signaling in *Pik3r1* LOF mice (Fig. S4, F and G) and normal response to glucose tolerance test (data not shown).

Further evidence for the critical role of the *PIK3R1* in non-immune tissues comes from analysis of SHORT syndrome, a multisystem order that is also caused by heterozygous autosomal dominant mutations in *PIK3R1* (Chudasama et al., 2013; Dyment et al., 2013; Thauvin-Robinet et al., 2013). Clinical features include those that define the acronym—*s*hort stature, *h*yperextensibility of joints, *o*cular depression, *R*ieger anomaly, and *t*eething delay—as well as lipoatrophy, insulin resistance, intrauterine growth restriction, and a characteristic facial gestalt (Avila et al., 2016). The *PIK3R1* mutations that cause SHORT syndrome are typically found in the inter-SH2 or C-terminal SH2 domains of p85α (Avila et al., 2016; Chudasama et al., 2013; Dyment et al., 2013; Thauvin-Robinet et al., 2013). Interestingly, several patients with APDS2 due to the canonical *PIK3R1* exon 11 skipping splice site mutations have also been described to have features of the SHORT syndrome (Bravo García-Morato et al., 2017; Petrovski et al., 2016; Ramirez et al., 2020), consistent with these mutations also affecting the inter-SH2 domain of p85. Notably, most of the patients reported here displayed at least some features of the SHORT syndrome (Table S1). Further, the body weight of our *Pik3r1* LOF mice was lower than WT controls (Fig. S4 E). This clearly demonstrates the importance of *PIK3R1* not only in immune cells but in other tissues, and indicates how dysregulated PI3K can lead to a broad clinical phenotype. However, further analysis will be required to determine the exact impacts of *PIK3R1* LOF in non-immune tissues.

Overall, our studies highlight the critical role of PI3K signaling in immune cell behavior but also demonstrate that this must be precisely and dynamically regulated to generate protective immune responses.

Materials and methods

Human blood and BM samples

Buffy coats were purchased from the Australian Red Cross Blood Service. BM was obtained from individuals undergoing lymphoma staging, and subsequently found to be uninvolved. Peripheral blood and BM were also collected from *PIK3R1* LOF patients. Patients in this study were consented on protocols approved by institutional human research ethics committees of St. Vincent's Hospital, The Children's Hospital at Westmead, Mayo Clinic, Royal Prince Alfred Hospital, Prince of Wales/Sydney Children's Hospital, Tehran University of Medical Sciences, and the National Institute of Allergy and Infectious Diseases Intramural Institutional Review Board. Some data from *PIK3CD* GOF patients presented in Fig. 1 is reproduced from our previously published studies (Avery et al., 2018; Bier et al., 2019; Edwards et al., 2019).

Human Abs

The following mAbs were used: anti-CD20 BUV395, anti-CD10 APC, anti-CD4 BUV737, anti-CD4 APCCy7, anti-CD25 PECy7, anti-CD27 PECy7, anti-CD27 PE, anti-CD45RA BV605, anti-CXCR5 A647, anti-IgG APC, anti-IgG PE, anti-IgG BV605, anti-CD8 BUV395, anti-PD1 BV605, Streptavidin-PerCPCy5.5, anti-IgM PerCPCy5.5, anti-CD3 BV421, anti-IL-2 BV711, anti-IL-9 PerCPCy5.5, anti-IL-13 BV421, anti-IL-17F BV786, anti-IFN-γ BV605, anti-TNF-α BUV395, anti-CD19 BV711, anti-CD34 FITC, anti-CCR6 PE (all from Becton Dickinson); anti-CCR7 PECy7, anti-CD127 BV650, anti-IL-17A APCCy7, anti-CD20 Pacific Blue, anti-FoxP3 PE, anti-CXCR3 BV421 (BioLegend); anti-CD45RA PerCPCy5.5 (eBioscience); anti-CCR7 FITC (R&D Systems); anti-IgA-biotin (SouthernBiotech); anti-IL-4 PECy7, anti-IL-21 e660, anti-IL-22 PE (Thermo Fisher Scientific).

Human lymphocyte phenotyping

Peripheral blood mononuclear cells (PBMCs) were incubated with mAbs to CD20, CD27, CD10, IgG, IgA, CD3, CD4, CD127,

CD25, CD8, CD45RA, CCR7, and FoxP3. The proportions of $CD20^+CD27^-CD10^+$ (transitional), $CD20^+CD27^-CD10^-$ (naïve), and $CD20^+CD27^+CD10^-$ (memory) B cells, the proportions of IgG^+ and IgA^+ memory B cells was determined by flow cytometry (LSRII Fortessa; Becton Dickinson) and analyzed using FlowJo software (Tree Star). Similarly, analysis of T cell subpopulations determined proportions of: $CD4^+$ and $CD8^+$ T cells; Tfh cells; Tregs; naïve ($CD45RA^+CCR7^-$), central memory ($CD45RA^-CCR7^+$), and $CD45RA^+$ or $CD45RA^-$ effector memory cells within the $CD4^+$ and $CD8^+$ compartments. Intracellular staining for FoxP3 was performed using the True-Nuclear Transcription Factor Buffer Set (BioLegend) according to the manufacturer's protocols. BM aspirates were incubated with mAbs against CD19, CD34, CD10, CD20, and IgM. Proportions of pro-B ($CD19^+CD34^+CD10^+$ $CD20^-IgM^-$), pre-BI ($CD19^+CD34^-CD10^+CD20^-IgM^-$), pre-BII ($CD19^+CD34^-CD10^+$ $CD20^{dim}IgM^-$), immature ($CD19^+CD34^-CD10^+CD20^+IgM^+$), and recirculating mature ($CD19^+CD34^-CD10^-CD20^+$) B cells were determined.

In vitro stimulation and analysis of human B cells

PBMCs were labeled with mAbs against CD20, CD10, CD27, and IgG, and sorted for naïve, transitional, $CD27^-$, or unswitched (IgG^-) memory B cells using the FACSAria III (Becton Dickinson), ensuring >98% purity of the recovered populations. Transitional, naïve, or unswitched memory B cells were cultured in 96-well round-bottom plates ($30–40 \times 10^3$ cells per well for CFSE analysis or 5×10^3 cells per well to determine Ig secretion). B cells were stimulated with 200 ng/ml CD40L cross-linked to 50 ng/ml HA Peptide mAb (R&D Systems) alone or together with 50 ng/ml IL-21 (PeproTech), 1 µg/ml CpG 2006 (Sigma-Aldrich), 0.05% heat-killed, or formalin-fixed *Staphylococcus aureus* Cowan I strain (SAC; Sigma-Aldrich). Varying doses of the PI3K p110δ-specific inhibitor leniolisib (Hoegenauer et al., 2017; Rao et al., 2017) and equivalent doses of DMSO were also added.

B cell viability was determined using the Zombie Aqua Viability dye (BioLegend) and proliferation was measured by CFSE (eBioscience) as described previously (Avery et al., 2010; Hodgkin et al., 1996). Secretion of IgM, IgG, and IgA by in vitro cultured human transitional, naïve, and memory B cells was determined using Ig heavy-chain specific ELISAs, as described previously (Avery et al., 2005).

Isolation and functional characterization of human T cells

Naïve and memory $CD4^+$ T cells were isolated by excluding Tregs ($CD25^{hi}CD127^{lo}$) and then sorting $CD45RA^+CCR7^+$ cells and $CD45RA^-CCR7^{+/-}$ cells, respectively, ensuring >98% purity of the recovered populations. Sorted naïve and memory $CD4^+$ T cells were cultured in 96-well round-bottom plates (40×10^3 cells/well) with TAE beads (anti-CD2/CD3/CD28; Miltenyi Biotech). After 5 d, supernatants were harvested to measure secretion of IL-4, IL-5, IL-13, IL-17A, IL-17F, IFN-γ, and TNF-α using cytometric bead arrays (Becton Dickinson). IL-22 secretion was measured by ELISA (PeproTech). Intracellular cytokine expression was determined following re-stimulation of cells with PMA and ionomycin with addition of Brefeldin A (10 µg/ml) after 2 h.

Validation of novel *PIK3R1* mutation

RNA was isolated from PBMCs using the RNeasy Mini Kit (QIAGEN). First-strand cDNA was synthesized using the SuperScript III First-Strand Synthesis System (Invitrogen). The region from exon 9 to 3′ UTR of *PIK3R1* was amplified using forward 5′-AGAAAACATTTGAAGCAGATGAA-3′ and reverse 5′-CAGTGACTGCTTCAGTTATCACG-3′ primers.

Mice

All experiments were approved by the Garvan Institute–St. Vincent's Animal Ethics Committee and The University of Sydney Animal Ethics Committee. Mice were bred and housed in specific pathogen–free conditions at Australian BioResources (Moss Vale) and the Garvan Institute Biological Testing Facility. *Pik3cd*^{E1020K} mice (referred to as *Pik3cd* GOF mice) have been previously described (Avery et al., 2018). These mice are heterozygous for a G-to-A base substitution, resulting in a Glu-to-Lys amino acid substitution in p110δ at amino acid residue 1020 (i.e., E1020K; corresponding to E1021K in human p110δ, the most common mutation identified in patients with *PIK3CD* GOF mutations). *Pik3r1*^{E11SpD} LOF mice (referred to as *Pik3r1* LOF mice) were produced by the Mouse Engineering Garvan/ABR facility using CRISPR/Cas9 gene targeting in C57BL/6JAusb mouse embryos. The single guide RNA was based on the target site at the 3′ end of exon 11 of *Pik3r1* (5′-GGAGTACACCGGTACTTCCC*AGG*-3′; protospacer-associated motif = italicized and underlined) and was microinjected into the nucleus and cytoplasm of C57BL/6J zygotes together with polyadenylated *Streptococcus pyogenes* Cas9 mRNA and a 150 base single-stranded, deoxy-oligonucleotide homologous recombination substrate carrying the G > C substitution in the exon 11 splice donor site (Lucas et al., 2014b). A founder mouse heterozygous for this single base substitution was obtained and the *Pik3r1* LOF mouse line was maintained on an inbred C57BL/6JAusb background. WT or *Pik3r1* LOF mice were crossed to HyHEL10-transgenic (SW_{HEL}) mice (Phan et al., 2003) on a CD45.1 congenic (*Ptprc*$^{a/a}$) background, heterozygous for Rag1 deficiency to generate WT SW_{HEL} or *Pik3r1* LOF SW_{HEL} mice. WT or *Pik3r1* LOF mice were crossed with OT-II (Barnden et al., 1998) mice to generate WT OT-II or *Pik3r1* LOF OT-II mice. For in vivo experiments, donor cells were adoptively transferred into 6–12-wk-old C57BL/6 (CD45.1 congenic) or *Sh2d1a* deficient (Czar et al., 2001; CD45.1 congenic) mice (herein referred SAP KO mice) purchased from Australian BioResources.

Flow cytometry of mouse cells

The following Abs were purchased from BD Biosciences: anti-CD43 PE (S7), anti-CD93 BV711 (clone 493-RUO), anti-CD8a Pacific Blue (53–6.7), anti-CD44 BV605 (IM7), anti- CD45R/B220 BV786, anti-CD19 BV510 (1D3), anti-TCR β chain APC (H57-597), anti-CD95 PE (Jo2), biotinylated anti-CD138 (281–2), anti-CD16/CD32 Fc block (2.4G2), anti-IgM PE (AF6-78), anti-PD-1 PE (J43), anti-CD3 PerCP-Cy5.5 (17A2), biotinylated anti-IgM (AF6-78), anti-IL-4 BV786 (11B11), anti-CD45.1 BV421 (A20); anti-CD45.2 BUV395 (104); anti-CD62L APC (MEL-14), anti-CD25 PE (PC61), anti-CD185 (CXCR5) purified (2G8), anti-CD184 (CXCR4) BV421, Streptavidin-BV605, Streptavidin-BUV395, and Streptavidin-BV711. The following were purchased from eBioscience: anti-

CD23 PECy7 (B3B4), anti-Vα2 FITC (B20.1); anti-CD45.1 FITC, PECy7, biotinylated (A20); anti-CD45.2 APC-eFluor 780, PerCp Cy5.5 (104), anti- CD45.1 PECy7 (A20); anti-CD62L FITC (MEL-14), anti-CD5 APC (53-7.3), anti-CD4 APC-e780 (RM4-5), anti-CD93 PE (AA4.1), anti-FoxP3 PE-Cy7 (FJK-16 s); anti-Vβ5.1/5.2 TCR PerCP-eFluor 710 (MR9-4), and Streptavidin-PE-Cy7. The following were purchased from BioLegend: anti-CD127 APC (A7R34), anti-IgD APC-Cy7 (11-26c.2a), anti-CD24 Pacific Blue (M1/69), anti-γδ TCR PE-Cy7 (GL3), anti-CD38 PE-Cy7 (90), anti-CD86 BV650 (GL-1), anti-CD93 PerCP-Cy5.5 (AA4.1), anti-CD21/35 Pacific Blue (7E9), anti-IFNγ PerCP-Cy5.5 (XMG1.2); anti-IL-2 Alexa Fluor 647 (JES6-5H4); anti-IL-5 BV421 (TRFK5); anti-TNFα PE (MP6-XT22); and anti-IL17A PE-Cy7 (TC11-1810.1). The following was purchased from Cell Signaling Technology: pS6 (D57.2.2E) AF488, APC.

In vitro culture of murine B cells

Spleens of *Pik3cd* GOF, *Pik3r1* LOF, and WT mice were harvested, and single-cell suspensions were prepared. Splenocytes were labeled with mAb against B220, CD21/35, CD23, and CD93, and follicular B cells ($B220^+$ $CD23^+$ $CD21^{int}$ $CD93^-$) were sorted using a FACSAria III (Beckton Dickinson). Purity of the recovered populations was typically >98%. Sorted follicular B cells were labeled with CellTrace Yellow and then cultured in 48-well plates in RPMI1640 (Life Technologies) supplemented with 10% heat-inactivated FCS (Life Technologies), 5×10^{-5} M 2-ME, 0.1 mM nonessential amino acids, 1 mM sodium pyruvate, 10 mM Hepes, 100 U/ml penicillin, 100 µg/ml Streptomycin, 100 µg/ml Noromycin (all from Sigma-Aldrich) at a density of 0.2×10^6 cells/ml. B cells were stimulated with 10 µg/ml anti-CD40 clone FGK4.5 (Enzo Live Sciences) alone or in combination with 10 ng/ml IL-4 (R & D Systems), or 10 µg/ml LPS (Sigma-Aldrich) alone or together with 0.5 ng/ml human TGFβ (Peprotec). After 4 d, cells were harvested, washed, and stained with Zombie Aqua Viability Dye (BioLegend). Cells were then surface stained with B220, fixed with 2% formaldehyde, and permeabilized with saponin. Permeabilized cells were stained with mAbs to IgG1, IgE, IgG2b, and IgG3, and analyzed by flow cytometry.

SW_{HEL} adoptive transfers

Donor SW_{HEL} *Pik3r1* LOF or WT spleen cells containing 3×10^4 HEL-binding B cells were injected i.v. into CD45.1 congenic C57BL/6 recipient mice along with 2×10^8 SRBCs conjugated to HEL2X (Brink et al., 2015). Recipient sera and spleens were harvested at the time points described. HELWT was purchased from Sigma-Aldrich and recombinant HEL protein (HEL2X) was produced as previously described (Brink et al., 2015). Anti-HEL Ab levels of the different Ig subclasses in the sera of recipient mice were analyzed by ELISA. 96-well ELISA plates were coated with WT HEL and bound serum Ig was detected using Ig heavy chain isotype-specific Ab from BD Biosciences: biotinylated anti-IgG1 (A85-1), biotinylated anti-IgG2a/c (R19-15), biotinylated anti-IgG2b (R12-3), biotinylated anti-IgG3 (R40-82), biotinylated anti-IgM (R6-60.2). Ig levels for each class were quantified against recombinant HyHEL10 standards (Brink et al., 2015).

SHM analysis

SHM in GC B cells was determined as previously described (Avery et al., 2018; Kane et al., 2016). Briefly, recipient spleens were harvested and stained for flow cytometry. Donor-derived IgM or $IgG1^+$ GC B cells were single cells sorted. The variable region of the SW_{HEL} Ig (HyHEL10) heavy chain regions was amplified by PCR. The final product was sequenced by GENEWIZ and analyzed.

Follicular B cell stimulation and phosphoprotein assessment

Splenocytes from *Pik3r1* LOF, *Pik3cd* GOF, or WT mice were stained for anti-CD3 PerCP-Cy5.5, anti-B220 BV786, anti-CD21 BV421, anti-BV711 CD93, anti-CD23 PE-Cy7. Follicular B cells were identified by being $CD3^-B220^+$ $CD93^-CD23^+CD21^+$. Sorted follicular B cells from either *Pik3r1* LOF, *Pik3cd* GOF or WT mice (100 µl at a density of 4×10^6 cells/ml) were plated in a 96-well flat-bottom cell culture plate (Falcon) in RPMI1640 (Life Technologies) supplemented with 10% heat-inactivated FCS (Life Technologies), 5×10^{-5} M 2-ME, 0.1 mM nonessential amino acids, 1 mM sodium pyruvate, 10 mM Hepes, 100 U/ml penicillin, 100 µg/ml Streptomycin, 100 µg/ml Noromycin (all from Sigma-Aldrich). Cells were rested for 30 min at the incubator. Unstimulated controls were harvested at the end of the resting period. Remaining wells received 100 µl of either media, media with purified anti-IgM (final concentration 10 µg/ml—SouthernBiotech) or media with anti-CD40 (final concentration 10 µg/ml—Enzo Life Sciences) and were cultured for additional 15 or 30 min.

For staining cells were harvested, transferred to a V bottom staining plate and fixed with 2% formaldehyde (20 min in the dark, room temperature). Following fixation, cells were washed and then permeabilized with ice-cold 90% methanol (30 min on ice). Cells were carefully washed and stained for intracellular phosphoantibodies in FACs buffer for 40 min, room temperature.

Milliplex assays were performed according to the manufacturer's instructions. Briefly, total cell lysates were prepared and relative levels of pAkt, pGSK3β, pmTOR, and pPTEN were determined using the Milliplex MAP Total Akt/mTOR Magnetic Bead 11-Plex Kit (Merck Millipore) together with a Bio-Plex MAGPIX system (#171015044) and Bio-Plex Pro-Wash Station (Biorad). Data was generated using Bio-Plex Manager MP and analyzed on the Bio-Plex Manager 6.1 software.

OT-II adoptive transfers

Spleens were harvested from donor OT-II *Pik3r1* LOF or OT-II WT mice and single-cell suspensions were prepared. The percentage of OT-II cells was quantified by FACs. 3×10^4 OT-II cells (200 µl) were injected i.v. into aged and sex-matched CD45.1 congenic C57BL/6 or SAP KO recipient mice. Recipient mice were immunized intraperitoneally with OVA in Alum (OVA-Alum; 1:1, OVA 1 mg/ml: Imject Alum Thermo Fisher Scientific). Recipient spleens were harvested on day 7 and the donor cells were identified based on the expression of CD45.2 and analyzed by flow cytometry. For the ex vivo cytokine expression, splenocytes (4×10^6 cells in a 48-well flat-bottom plate) were stimulated with PMA (50 ng/ml) and ionomycin (375 ng/ml) for

6 h. Brefeldin A (10 µg/ml) was added to each well at 2 h of culture. Cells were then harvested, washed, and stained with Zombie Aqua (previously described) followed by CD4, CD45.1, and CD45.2 surface stain. Cells were fixed with 2% formalin and stained for intracellular cytokines as described previously. Anti-OVA IgM Ab levels in the sera of recipient mice were analyzed by ELISA. 96-well ELISA plates were coated with OVA and bound serum Ig was detected using IgM heavy chain isotype specific Ab (BD Biosciences; biotinylated anti-IgM [R6-60.2]). IgM levels for were normalized to pooled sera from mice previously immunized with OVA.

In vitro T cell polarizing cultures

Splenocytes from *Pik3r1* LOF, *Pik3cd* GOF, or WT mice were stained for anti-CD3 PerCP-Cy5.5, anti-B220 BV786, anti-CD44 FITC, anti-CD62L PE, anti-CD8α Pacific Blue, anti-CD4 APCe780, anti-γδTCR PE-Cy7. Naïve $CD4^+$T cells were identified by being $CD3^+B220^-$ $\gamma\delta TCR^-CD4^+CD8^-CD62L^{hi}CD44^{lo}$. Sorted *Pik3r1* LOF, *Pik3cd* GOF, or WT naïve $CD4^+$T cells were cultured in flat-bottom 96-well plates previously coated overnight with anti-CD3 (4 mg/ml; BioLegend) in 1xPBS (Gibco). $CD4^+$ naïve T cells were cultured in RPMI 1640 (Life Technologies) supplemented with 10% heat-inactivated FCS (Life Technologies), 5×10^{-5} mol/l 2-mercapotoethanol, 0.1 mM nonessential amino acids, 1 mM sodium pyruvate, 10 mM Hepes, 100 U/ml penicillin, 100 µg/ml streptomycin, and 100 µg/ml noromycin (all from Sigma-Aldrich) for 4 d at a density of 0.5×10^6 cells/ml in the following conditions: Th0 (anti-CD28 1 µg/ml, anti-IL-4 5 µg/ml, anti-IFNγ 5 µg/ml); Th1 (anti-CD28 1 µg/ml, anti-IL-4 5 µg/ml, IL-12 10 ng/ml); Th2 (anti-CD28 1 µg/ml, IL-4 10 ng/ml, anti-IFNγ 5 µg/ml); Th17 (anti-CD28 1 µg/ml, IL-6 20 ng/ml, human TGFβ 1 ng/ml, anti-IFNγ 5 µg/ml, anti-IL-4 5 µg/ml). After 4 d of culture, cells were stimulated with PMA (50 ng/ml) and ionomycin (375 ng/ml) for 6 h. Brefeldin A (10 mg/ml) was added to each well 2 h after the addition of PMA/ionomycin. Cells were then harvested, washed, and stained with Zombie Aqua Viability Dye (BioLegend). $CD4^+$ T cells were fixed with 2% formalin; permeabilized with saponin (0.1%); stained intracellularly with mAbs directed against TNFα, IFNγ, IL17A, IL5; and analyzed by flow cytometry.

Fat explant Western blots

Mice were euthanized through cervical dislocation and epididymal white adipose tissue was excised from the mice. Explants were prepared as described previously (Nelson et al., 2022). Briefly, adipose tissue was finely chopped in DMEM containing 25 mM Hepes and 2% BSA, washed three times, split into two tubes, and then basaled for 2 h with shaking in a 37°C waterbath. Adipose explants were then either incubated with PBS or 10 nM insulin in PBS for 20 min. Signaling was stopped by adding ice-cold PBS directly to the tubes and then washing the explants three times in ice-cold PBS on ice. Samples were prepared as described previously (Humphrey et al., 2018). Briefly, the explants were lysed in 4% sodium deoxycholate 100 mM Tris-HCl, pH 8.5, heated immediately to 95°C for 5 min, sonicated and centrifuged at 13,000 × *g* for 10 min at 4°C. The fat layer was removed and samples were quantified by BCA protein assay. Samples were made up in 1X laemmli buffer containing TCEP and loaded onto 9% SDS-page gel before being transferred to a polyvinylidene difluoride membrane. Abs against Akt S473, Akt T308, and pan-Akt were purchased from Cell Signaling Technologies. Pan-14-3-3 Ab was purchased from Santa Cruz Biotechnology. Membranes were incubated in primary Ab in 5% BSA tris-buffered saline - tween (TBS-T) overnight, washed in TBS-T three times, incubated in secondary Ab (LI-COR, Inc.) in 5% milk in TBS-T for 1 h at room temperature, washed with TBS-T three times, and then imaged on the LI-COR Odyssey (LI-COR, Inc.).

Statistical analysis

Significant differences were determined using Prism (GraphPad Software). Asterisks indicate statistical significance (*, $P < 0.05$; **, $P < 0.01$; ***, $P < 0.001$; ****, $P < 0.0001$).

Online supplemental material

Fig. S1 shows further analysis of cells from *PIK3R1* LOF patients. Fig. S2 shows further phenotyping of the *Pik3r1* LOF mouse. Fig. S3 shows further responses of pik3r1 LOF $CD4^+$ T cells and B cells. Fig. S3 shows analysis of B cell signaling and non-immune phenotypes in *Pik3r1* LOF and Pik3cd GOF mice. Table S1 shows *PIK3R1* LOF patient cohort clinical, genetic, and demographic information.

Data availability

The data are available from the corresponding author upon reasonable request.

Acknowledgments

We thank the patients and their families for their invaluable contributions to this project. We are also grateful to the Garvan Flow Cytometry facility for cell sorting.

This work was supported by program grants (1113904 to S.G. Tangye, R. Brink), project grant (1127157 to S.G. Tangye, E.K. Deenick, C.S. Ma), Principal Research Fellowship (1042925 to S.G. Tangye), and a Leadership 3 Investigator Grant (1176665 to S.G. Tangye) awarded by the National Health and Medical Research Council. J. Bier was supported through the American Association of Immunologists Careers in Immunology Fellowship Program. D.E. James is an Australian Research Council Laureate Fellow. Clinical Immunogenomics Research Consortium Australasia is supported by the Jeffrey Modell Foundation, Sydney Partnership for Health, Education, Research and Enterprise Triple I Clinical Academic Group, University of New South Wales Medicine Infection, Immunology and Inflammation Theme, and the John Brown Cook Foundation.

Author contributions: T. Nguyen, A. Lau, J. Bier, D.T. Avery, K.C. Cooke, H. Lenthall, S. Ruiz-Diaz, and H. Brigden performed experiments and analyzed data; W.A. Sewell provided normal bone marrow samples; L. Droney, S. Okada, T. Asano, H. Abolhassani, Z. Chavoshzadeh, R.S. Abraham, N. Rajapakse, E.W. Klee, J.A. Church, A. Williams, M. Wong, and G. Uzel provided clinical details and patient samples; C. Burkhart provided p110δ inhibitors; D. Zahra and R. Brink generated the *Pik3cd* GOF and *Pik3r1* LOF mice; D.R. Croucher, D.E. James, C.S. Ma, S.G. Tangye,

and E.K. Deenick supervised experiments; S.G. Tangye and E.K. Deenick designed and supervised the project; T. Nguyen, A. Lau, J. Bier, S.G. Tangye, and E.K. Deenick interpreted the data and wrote the paper. All authors edited the manuscript.

Disclosures: A. Lau reported being an employee of AstraZeneca since January 2023. J. Bier reported being an employee of Takeda Pharmaceutical since September 2022. R.S. Abraham reported personal fees from Enzyvant Therapeutics, Horizon Pharma, Beckman Coulter, and ClinGen outside the submitted work. C. Burkhart reported being an employee and shareholder of Novartis Pharma AG. Leniolisib is a p110δ-specific inhibitor and was discovered and developed by Novartis Pharma AG. Leniolisib was provided in 2016 to S.G. Tangye for studies described in the manuscript. Leniolisib was outlicensed to Pharming Group N.V. in 2019. S.G. Tangye reported being on the Pharming Group NV Global Advisory Board for the use of leniolisib to treat individuals with inborn errors of immunity due to mutations in PIK3CD or PIK3R1. Pharming has licensed leniolisib from Novartis as a therapy for these conditions. E.K. Deenick reported "other" from CSL outside the submitted work. No other disclosures were reported.

Submitted: 14 June 2022
Revised: 22 December 2022
Accepted: 27 February 2023

References

Acosta-Rodríguez, E.V., L. Rivino, J. Geginat, D. Jarrossay, M. Gattorno, A. Lanzavecchia, F. Sallusto, and G. Napolitani. 2007. Surface phenotype and antigenic specificity of human interleukin 17-producing T helper memory cells. *Nat. Immunol.* 8:639–646. https://doi.org/10.1038/ni1467

Al Qureshah, F., S. Sagadiev, C.D. Thouvenel, S. Liu, Z. Hua, B. Hou, M. Acharya, R.G. James, and D.J. Rawlings. 2021. Activated PI3Kδ signals compromise plasma cell survival via limiting autophagy and increasing ER stress. *J. Exp. Med.* 218:218. https://doi.org/10.1084/jem.20211035

Angulo, I., O. Vadas, F. Garçon, E. Banham-Hall, V. Plagnol, T.R. Leahy, H. Baxendale, T. Coulter, J. Curtis, C. Wu, et al. 2013. Phosphoinositide 3-kinase δ gene mutation predisposes to respiratory infection and airway damage. *Science.* 342:866–871. https://doi.org/10.1126/science.1243292

Asano, T., S. Okada, M. Tsumura, T.W. Yeh, K. Mitsui-Sekinaka, Y. Tsujita, Y. Ichinose, A. Shimada, K. Hashimoto, T. Wada, et al. 2018. Enhanced AKT phosphorylation of circulating B cells in patients with activated PI3Kδ syndrome. *Front. Immunol.* 9:568. https://doi.org/10.3389/fimmu.2018.00568

Avery, D.T., E.K. Deenick, C.S. Ma, S. Suryani, N. Simpson, G.Y. Chew, T.D. Chan, U. Palendira, J. Bustamante, S. Boisson-Dupuis, et al. 2010. B cell-intrinsic signaling through IL-21 receptor and STAT3 is required for establishing long-lived antibody responses in humans. *J. Exp. Med.* 207:155–171. https://doi.org/10.1084/jem.20091706

Avery, D.T., J.I. Ellyard, F. Mackay, L.M. Corcoran, P.D. Hodgkin, and S.G. Tangye. 2005. Increased expression of CD27 on activated human memory B cells correlates with their commitment to the plasma cell lineage. *J. Immunol.* 174:4034–4042. https://doi.org/10.4049/jimmunol.174.7.4034

Avery, D.T., A. Kane, T. Nguyen, A. Lau, A. Nguyen, H. Lenthall, K. Payne, W. Shi, H. Brigden, E. French, et al. 2018. Germline-activating mutations in *PIK3CD* compromise B cell development and function. *J. Exp. Med.* 215:2073–2095. https://doi.org/10.1084/jem.20180010

Avila, M., D.A. Dyment, J.V. Sagen, J. St-Onge, U. Moog, B.H.Y. Chung, S. Mo, S. Mansour, A. Albanese, S. Garcia, et al. 2016. Clinical reappraisal of SHORT syndrome with *PIK3R1* mutations: Toward recommendation for molecular testing and management. *Clin. Genet.* 89:501–506. https://doi.org/10.1111/cge.12688

Barnden, M.J., J. Allison, W.R. Heath, and F.R. Carbone. 1998. Defective TCR expression in transgenic mice constructed using cDNA-based alpha- and beta-chain genes under the control of heterologous regulatory elements. *Immunol. Cell Biol.* 76:34–40. https://doi.org/10.1046/j.1440-1711.1998.00709.x

Bier, J., and E.K. Deenick. 2022. The role of dysregulated PI3Kdelta signaling in human autoimmunity. *Immunol. Rev.* 307:134–144. https://doi.org/10.1111/imr.13067

Bier, J., G. Rao, K. Payne, H. Brigden, E. French, S.J. Pelham, A. Lau, H. Lenthall, E.S.J. Edwards, J.M. Smart, et al. 2019. Activating mutations in *PIK3CD* disrupt the differentiation and function of human and murine $CD4^+$ T cells. *J. Allergy Clin. Immunol.* 144:236–253. https://doi.org/10.1016/j.jaci.2019.01.033

Bilanges, B., Y. Posor, and B. Vanhaesebroeck. 2019. PI3K isoforms in cell signalling and vesicle trafficking. *Nat. Rev. Mol. Cell Biol.* 20:515–534. https://doi.org/10.1038/s41580-019-0129-z

Bravo García-Morato, M., S. García-Miñaúr, J. Molina Garicano, F. Santos Simarro, L. Del Pino Molina, E. López-Granados, A. Ferreira Cerdán, and R. Rodríguez Pena. 2017. Mutations in *PIK3R1* can lead to APDS2, SHORT syndrome or a combination of the two. *Clin. Immunol.* 179:77–80. https://doi.org/10.1016/j.clim.2017.03.004

Brink, R., and T.G. Phan. 2018. Self-Reactive B cells in the germinal center reaction. *Annu. Rev. Immunol.* 36:339–357. https://doi.org/10.1146/annurev-immunol-051116-052510

Brink, R., D. Paus, K. Bourne, J.R. Hermes, S. Gardam, T.G. Phan, and T.D. Chan. 2015. The SW(HEL) system for high-resolution analysis of in vivo antigen-specific T-dependent B cell responses. *Methods Mol. Biol.* 1291:103–123. https://doi.org/10.1007/978-1-4939-2498-1_9

Brodsky, N.N., and C.L. Lucas. 2021. Infections in activated PI3K delta syndrome (APDS). *Curr. Opin. Immunol.* 72:146–157. https://doi.org/10.1016/j.coi.2021.04.010

Cannons, J.L., S. Preite, S.M. Kapnick, G. Uzel, and P.L. Schwartzberg. 2018. Genetic defects in phosphoinositide 3-kinase δ influence $CD8^+$ T cell survival, differentiation, and function. *Front. Immunol.* 9:1758. https://doi.org/10.3389/fimmu.2018.01758

Chantry, D., A. Vojtek, A. Kashishian, D.A. Holtzman, C. Wood, P.W. Gray, J.A. Cooper, and M.F. Hoekstra. 1997. p110delta, a novel phosphatidylinositol 3-kinase catalytic subunit that associates with p85 and is expressed predominantly in leukocytes. *J. Biol. Chem.* 272:19236–19241. https://doi.org/10.1074/jbc.272.31.19236

Chudasama, K.K., J. Winnay, S. Johansson, T. Claudi, R. König, I. Haldorsen, B. Johansson, J.R. Woo, D. Aarskog, J.V. Sagen, et al. 2013. SHORT syndrome with partial lipodystrophy due to impaired phosphatidylinositol 3 kinase signaling. *Am. J. Hum. Genet.* 93:150–157. https://doi.org/10.1016/j.ajhg.2013.05.023

Crotty, S., E.N. Kersh, J. Cannons, P.L. Schwartzberg, and R. Ahmed. 2003. SAP is required for generating long-term humoral immunity. *Nature.* 421:282–287. https://doi.org/10.1038/nature01318

Czar, M.J., E.N. Kersh, L.A. Mijares, G. Lanier, J. Lewis, G. Yap, A. Chen, A. Sher, C.S. Duckett, R. Ahmed, and P.L. Schwartzberg. 2001. Altered lymphocyte responses and cytokine production in mice deficient in the X-linked lymphoproliferative disease gene SH2D1A/DSHP/SAP. *Proc. Natl. Acad. Sci. USA.* 98:7449–7454. https://doi.org/10.1073/pnas.131193098

Deau, M.-C., L. Heurtier, P. Frange, F. Suarez, C. Bole-Feysot, P. Nitschke, M. Cavazzana, C. Picard, A. Durandy, A. Fischer, et al. 2014. A human immunodeficiency caused by mutations in the *PIK3R1* gene. *J. Clin. Invest.* 124:3923–3928. https://doi.org/10.1172/JCI75746

Deenick, E.K., D.T. Avery, A. Chan, L.J. Berglund, M.L. Ives, L. Moens, J.L. Stoddard, J. Bustamante, S. Boisson-Dupuis, M. Tsumura, et al. 2013. Naive and memory human B cells have distinct requirements for STAT3 activation to differentiate into antibody-secreting plasma cells. *J. Exp. Med.* 210:2739–2753. https://doi.org/10.1084/jem.20130323

Deenick, E.K., J. Hasbold, and P.D. Hodgkin. 1999. Switching to IgG3, IgG2b, and IgA is division linked and independent, revealing a stochastic framework for describing differentiation. *J. Immunol.* 163:4707–4714. https://doi.org/10.4049/jimmunol.163.9.4707

Deenick, E.K., and C.S. Ma. 2011. The regulation and role of T follicular helper cells in immunity. *Immunology.* 134:361–367. https://doi.org/10.1111/j.1365-2567.2011.03487.x

Dominguez-Sola, D., J. Kung, A.B. Holmes, V.A. Wells, T. Mo, K. Basso, and R. Dalla-Favera. 2015. The FOXO1 transcription factor instructs the germinal center dark zone program. *Immunity.* 43:1064-1074. https://doi.org/10.1016/j.immuni.2015.10.015

Dornan, G.L., B.D. Siempelkamp, M.L. Jenkins, O. Vadas, C.L. Lucas, and J.E. Burke. 2017. Conformational disruption of PI3Kδ regulation by immunodeficiency mutations in *PIK3CD* and *PIK3R1*. *Proc. Natl. Acad. Sci. USA.* 114:1982–1987. https://doi.org/10.1073/pnas.1617244114

Dulau Florea, A.E., R.C. Braylan, K.T. Schafernak, K.W. Williams, J. Daub, R.K. Goyal, J.M. Puck, V.K. Rao, S. Pittaluga, S.M. Holland, et al. 2017. Abnormal B-cell maturation in the bone marrow of patients with germline mutations in *PIK3CD*. *J. Allergy Clin. Immunol.* 139:1032–1035.e6. https://doi.org/10.1016/j.jaci.2016.08.028

Dyment, D.A., A.C. Smith, D. Alcantara, J.A. Schwartzentruber, L. Basel-Vanagaite, C.J. Curry, I.K. Temple, W. Reardon, S. Mansour, M.R. Haq, et al. 2013. Mutations in *PIK3R1* cause SHORT syndrome. *Am. J. Hum. Genet.* 93:158–166. https://doi.org/10.1016/j.ajhg.2013.06.005

Edwards, E.S.J., J. Bier, T.S. Cole, M. Wong, P. Hsu, L.J. Berglund, K. Boztug, A. Lau, E. Gostick, D.A. Price, et al. 2019. Activating *PIK3CD* mutations impair human cytotoxic lymphocyte differentiation and function and EBV immunity. *J. Allergy Clin. Immunol.* 143:276–291.e6. https://doi.org/10.1016/j.jaci.2018.04.030

Elkaim, E., B. Neven, J. Bruneau, K. Mitsui-Sekinaka, A. Stanislas, L. Heurtier, C.L. Lucas, H. Matthews, M.-C. Deau, S. Sharapova, et al. 2016. Clinical and immunologic phenotype associated with activated phosphoinositide 3-kinase δ syndrome 2: A cohort study. *J. Allergy Clin. Immunol.* 138: 210–218.e9. https://doi.org/10.1016/j.jaci.2016.03.022

Fruman, D.A., H. Chiu, B.D. Hopkins, S. Bagrodia, L.C. Cantley, and R.T. Abraham. 2017. The PI3K pathway in human disease. *Cell*. 170:605–635. https://doi.org/10.1016/j.cell.2017.07.029

Fruman, D.A., F. Mauvais-Jarvis, D.A. Pollard, C.M. Yballe, D. Brazil, R.T. Bronson, C.R. Kahn, and L.C. Cantley. 2000. Hypoglycaemia, liver necrosis and perinatal death in mice lacking all isoforms of phosphoinositide 3-kinase p85 alpha. *Nat. Genet.* 26:379–382. https://doi.org/10.1038/81715

Hodgkin, P.D., J.H. Lee, and A.B. Lyons. 1996. B cell differentiation and isotype switching is related to division cycle number. *J. Exp. Med.* 184: 277–281. https://doi.org/10.1084/jem.184.1.277

Hoegenauer, K., N. Soldermann, F. Zécri, R.S. Strang, N. Graveleau, R.M. Wolf, N.G. Cooke, A.B. Smith, G.J. Hollingworth, J. Blanz, et al. 2017. Discovery of CDZ173 (Leniolisib), representing a structurally novel class of PI3K delta-selective inhibitors. *ACS Med. Chem. Lett.* 8:975–980. https://doi.org/10.1021/acsmedchemlett.7b00293

Humphrey, S.J., O. Karayel, D.E. James, and M. Mann. 2018. High-throughput and high-sensitivity phosphoproteomics with the EasyPhos platform. *Nat. Protoc.* 13:1897–1916. https://doi.org/10.1038/s41596-018-0014-9

Jamee, M., S. Moniri, M. Zaki-Dizaji, P. Olbrich, R. Yazdani, F. Jadidi-Niaragh, F. Aghamahdi, H. Abolhassani, A.M. Condliffe, A. Aghamohammadi, and G. Azizi. 2019. Clinical, immunological, and genetic features in patients with activated PI3Kδ syndrome (APDS): A systematic review. *Clin. Rev. Allergy Immunol.* 59:323–333. https://doi.org/10.1007/s12016-019-08738-9

Jia, Y., Q. Yang, Y. Wang, W. Li, X. Chen, T. Xu, Z. Tian, M. Feng, L. Zhang, W. Tang, et al. 2021. Hyperactive PI3Kδ predisposes naive T cells to activation via aerobic glycolysis programs. *Cell. Mol. Immunol.* 18:1783–1797. https://doi.org/10.1038/s41423-020-0379-x

Kane, A., A. Lau, R. Brink, S.G. Tangye, and E.K. Deenick. 2016. B-cell-specific STAT3 deficiency: Insight into the molecular basis of autosomal-dominant hyper-IgE syndrome. *J. Allergy Clin. Immunol.* 138:1455–1458.e3. https://doi.org/10.1016/j.jaci.2016.05.018

Lau, A., D.T. Avery, K. Jackson, H. Lenthall, S. Volpi, H. Brigden, A.J. Russell, J. Bier, J.H. Reed, J.M. Smart, et al. 2020. Activated PI3Kδ breaches multiple B cell tolerance checkpoints and causes autoantibody production. *J. Exp. Med.* 217:45. https://doi.org/10.1084/jem.20191336

Lucas, C.L., H.S. Kuehn, F. Zhao, J.E. Niemela, E.K. Deenick, U. Palendira, D.T. Avery, L. Moens, J.L. Cannons, M. Biancalana, et al. 2014a. Dominant-activating germline mutations in the gene encoding the PI(3)K catalytic subunit p110δ result in T cell senescence and human immunodeficiency. *Nat. Immunol.* 15:88–97. https://doi.org/10.1038/ni.2771

Lucas, C.L., Y. Zhang, A. Venida, Y. Wang, J. Hughes, J. McElwee, M. Butrick, H. Matthews, S. Price, M. Biancalana, et al. 2014b. Heterozygous splice mutation in PIK3R1 causes human immunodeficiency with lymphoproliferation due to dominant activation of PI3K. *J. Exp. Med.* 211: 2537–2547. https://doi.org/10.1084/jem.20141759

Ma, C.S., N. Wong, G. Rao, D.T. Avery, J. Torpy, T. Hambridge, J. Bustamante, S. Okada, J.L. Stoddard, E.K. Deenick, et al. 2015. Monogenic mutations differentially affect the quantity and quality of T follicular helper cells in patients with human primary immunodeficiencies. *J. Allergy Clin. Immunol.* 136:993–1006.e1. https://doi.org/10.1016/j.jaci.2015.05.036

Maccari, M.E., H. Abolhassani, A. Aghamohammadi, A. Aiuti, O. Aleinikova, C. Bangs, S. Baris, F. Barzaghi, H. Baxendale, M. Buckland, et al. 2018. Disease evolution and response to rapamycin in activated phosphoinositide 3-kinase δ syndrome: The European society for immunodeficiencies-activated phosphoinositide 3-kinase δ syndrome registry. *Front. Immunol.* 9:543. https://doi.org/10.3389/fimmu.2018.00543

Morita, R., N. Schmitt, S.E. Bentebibel, R. Ranganathan, L. Bourdery, G. Zurawski, E. Foucat, M. Dullaers, S. Oh, N. Sabzghabaei, et al. 2011. Human blood CXCR5(+)CD4(+) T cells are counterparts of T follicular cells and contain specific subsets that differentially support antibody secretion. *Immunity*. 34:108–121. https://doi.org/10.1016/j.immuni.2010.12.012

Nelson, M.E., S. Madsen, K.C. Cooke, A.M. Fritzen, I.H. Thorius, S.W.C. Masson, L. Carroll, F.C. Weiss, M.M. Seldin, M. Potter, et al. 2022. Systems-level analysis of insulin action in mouse strains provides insight into tissue- and pathway-specific interactions that drive insulin resistance. *Cell Metab.* 34:227–239.e6. https://doi.org/10.1016/j.cmet.2021.12.013

Okkenhaug, K. 2013. Signaling by the phosphoinositide 3-kinase family in immune cells. *Annu. Rev. Immunol.* 31:675–704. https://doi.org/10.1146/annurev-immunol-032712-095946

Paus, D., T.G. Phan, T.D. Chan, S. Gardam, A. Basten, and R. Brink. 2006. Antigen recognition strength regulates the choice between extrafollicular plasma cell and germinal center B cell differentiation. *J. Exp. Med.* 203:1081–1091. https://doi.org/10.1084/jem.20060087

Petrovski, S., R.E. Parrott, J.L. Roberts, H. Huang, J. Yang, B. Gorentla, T. Mousallem, E. Wang, M. Armstrong, D. McHale, et al. 2016. Dominant splice site mutations in *PIK3R1* cause hyper IgM syndrome, lymphadenopathy and short stature. *J. Clin. Immunol.* 36:462–471. https://doi.org/10.1007/s10875-016-0281-6

Phan, T.G., M. Amesbury, S. Gardam, J. Crosbie, J. Hasbold, P.D. Hodgkin, A. Basten, and R. Brink. 2003. B cell receptor-independent stimuli trigger immunoglobulin (Ig) class switch recombination and production of IgG autoantibodies by anergic self-reactive B cells. *J. Exp. Med.* 197:845–860. https://doi.org/10.1084/jem.20022144

Phan, T.G., D. Paus, T.D. Chan, M.L. Turner, S.L. Nutt, A. Basten, and R. Brink. 2006. High affinity germinal center B cells are actively selected into the plasma cell compartment. *J. Exp. Med.* 203:2419–2424. https://doi.org/10.1084/jem.20061254

Preite, S., J.L. Cannons, A.J. Radtke, I. Vujkovic-Cvijin, J. Gomez-Rodriguez, S. Volpi, B. Huang, J. Cheng, N. Collins, J. Reilley, et al. 2018a. Hyperactivated PI3Kδ promotes self and commensal reactivity at the expense of optimal humoral immunity. *Nat. Immunol.* 19:986–1000. https://doi.org/10.1038/s41590-018-0182-3

Preite, S., J. Gomez-Rodriguez, J.L. Cannons, and P.L. Schwartzberg. 2019. T and B-cell signaling in activated PI3K delta syndrome: From immunodeficiency to autoimmunity. *Immunol. Rev.* 291:154–173. https://doi.org/10.1111/imr.12790

Preite, S., B. Huang, J.L. Cannons, D.B. McGavern, and P.L. Schwartzberg. 2018b. PI3K orchestrates T follicular helper cell differentiation in a context dependent manner: Implications for autoimmunity. *Front. Immunol.* 9:3079. https://doi.org/10.3389/fimmu.2018.03079

Ramirez, L., W. Tamayo, and H. Ale. 2020. APDS2 and SHORT syndrome in a teenager with *PIK3R1* pathogenic variant. *J. Clin. Immunol.* 40: 1020–1025. https://doi.org/10.1007/s10875-020-00843-1

Rao, V.K., S. Webster, V.A.S.H. Dalm, A. Šedivá, P.M. van Hagen, S. Holland, S.D. Rosenzweig, A.D. Christ, B. Sloth, M. Cabanski, et al. 2017. Effective "activated PI3Kδ syndrome"-targeted therapy with the PI3Kδ inhibitor leniolisib. *Blood*. 130:2307–2316. https://doi.org/10.1182/blood-2017-08-801191

Recher, M., L.J. Berglund, D.T. Avery, M.J. Cowan, A.R. Gennery, J. Smart, J. Peake, M. Wong, S.-Y. Pai, S. Baxi, et al. 2011. IL-21 is the primary common γ chain-binding cytokine required for human B-cell differentiation in vivo. *Blood*. 118:6824–6835. https://doi.org/10.1182/blood-2011-06-362533

Sander, S., V.T. Chu, T. Yasuda, A. Franklin, R. Graf, D.P. Calado, S. Li, K. Imami, M. Selbach, M. Di Virgilio, et al. 2015. PI3 kinase and FOXO1 transcription factor activity differentially control B cells in the germinal center light and dark zones. *Immunity*. 43:1075–1086. https://doi.org/10.1016/j.immuni.2015.10.021

Stark, A.-K., A. Chandra, K. Chakraborty, R. Alam, V. Carbonaro, J. Clark, S. Sriskantharajah, G. Bradley, A.G. Richter, E. Banham-Hall, et al. 2018. PI3Kδ hyper-activation promotes development of B cells that exacerbate *Streptococcus pneumoniae* infection in an antibody-independent manner. *Nat. Commun.* 9:3174. https://doi.org/10.1038/s41467-018-05674-8

Tangye, S.G., C.S. Ma, R. Brink, and E.K. Deenick. 2013. The good, the bad and the ugly: TFH cells in human health and disease. *Nat. Rev. Immunol.* 13: 412–426. https://doi.org/10.1038/nri3447

Thauvin-Robinet, C., M. Auclair, L. Duplomb, M. Caron-Debarle, M. Avila, J. St-Onge, M. Le Merrer, B. Le Luyer, D. Héron, M. Mathieu-Dramard, et al. 2013. *PIK3R1* mutations cause syndromic insulin resistance with lipoatrophy. *Am. J. Hum. Genet.* 93:141–149. https://doi.org/10.1016/j.ajhg.2013.05.019

Thouenon, R., N. Moreno-Corona, L. Poggi, A. Durandy, and S. Kracker. 2021. Activated PI3Kinase delta syndrome-A multifaceted disease. *Front Pediatr.* 9:652405. https://doi.org/10.3389/fped.2021.652405

Vazquez, F., S. Ramaswamy, N. Nakamura, and W.R. Sellers. 2000. Phosphorylation of the PTEN tail regulates protein stability and function. *Mol. Cell. Biol.* 20:5010–5018. https://doi.org/10.1128/MCB.20.14.5010-5018.2000

Wentink, M.W.J., Y.M. Mueller, V.A.S.H. Dalm, G.J. Driessen, P.M. van Hagen, J.M. van Montfrans, M. van der Burg, and P.D. Katsikis. 2018. Exhaustion of the $CD8^+$ T cell compartment in patients with mutations in phosphoinositide 3-kinase delta. *Front. Immunol.* 9:446. https://doi.org/10.3389/fimmu.2018.00446

Wray-Dutra, M.N., F. Al Qureshah, G. Metzler, M. Oukka, R.G. James, and D.J. Rawlings. 2018. Activated *PIK3CD* drives innate B cell expansion yet limits B cell-intrinsic immune responses. *J. Exp. Med.* 215:2485–2496. https://doi.org/10.1084/jem.20180617

Supplemental material

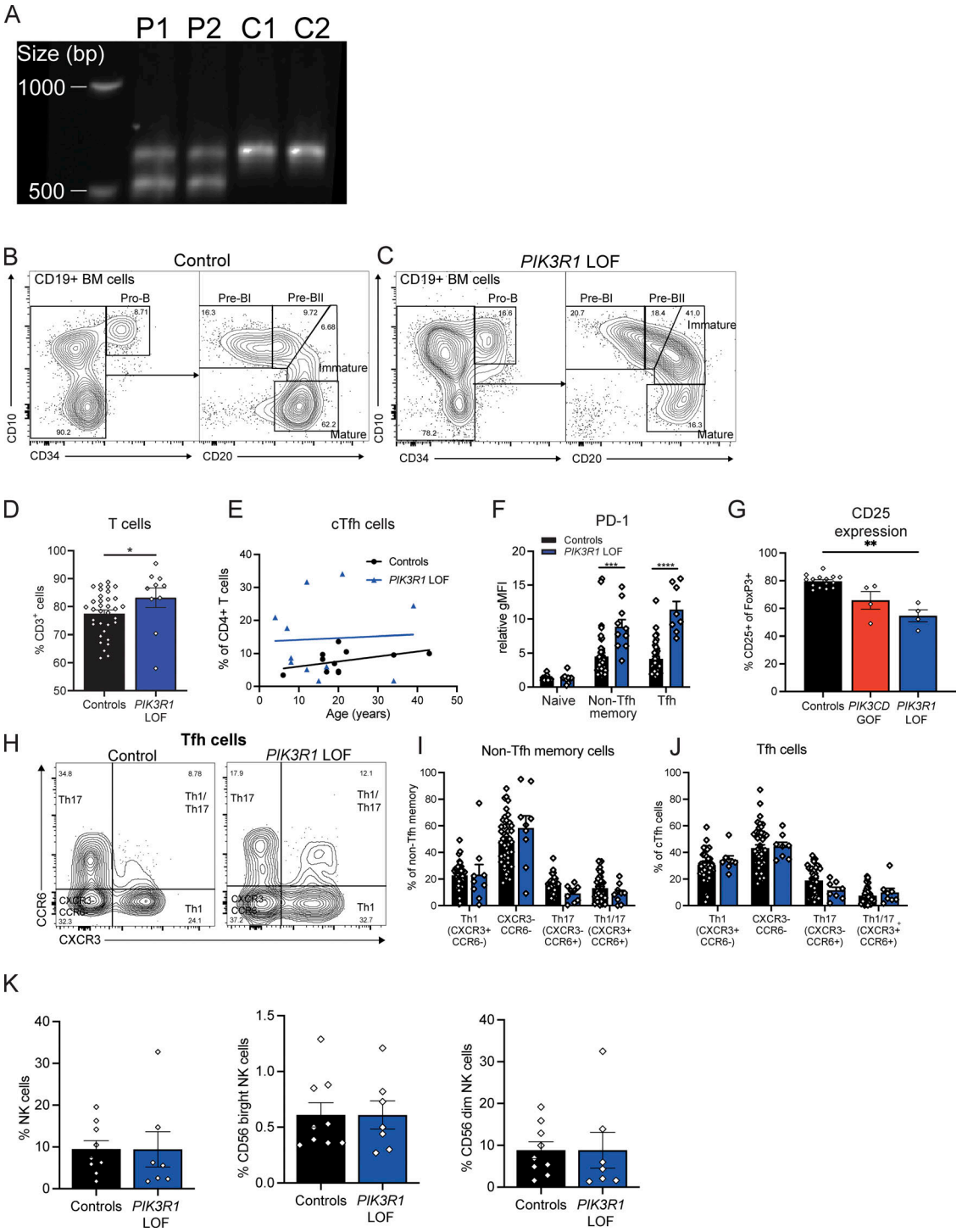

Figure S1. **Extended phenotyping of *PIK3R1* LOF patients. (A)** PCR for exon 11 flanking region of *PIK3R1* was performed on cDNA from healthy donors (C1, 2) and *PIK3R1* LOF PBMCs (P1, 2). **(B and C)** Mononuclear cells isolated from BM aspirates of healthy donors (n = 9), *PIK3R1* LOF (n = 2), *PIK3CD* GOF (n = 3), and X-linked agammaglobulinemia (n = 1) patients were stained to identify distinct B cell subpopulations. Contour plots show CD34 versus CD10 staining used to identify pro-B cells in (B) a representative healthy donor and (C) a *PIK3R1* LOF patient. B cells were further analyzed by CD10 and CD20 to identify pro-B, pre-BI, pre-BII, immature, and recirculating mature B cells. **(D–J)** PBMCs from healthy controls (n = 11–42) and *PIK3R1* LOF patients (n = 4–10) were stained to determine (D) proportion of T cells ($CD3^+$) within the lymphocyte population, (E) percentage of cTfh cells at different ages, (F) expression of PD-1 on naïve, non-Tfh memory, and Tfh cells. The $CD4^+$ T cell compartment was also analyzed for percentage of (G) $CD25^+$ cells within the $CD4^+FoxP3^+$ Treg population. **(H)** CXCR3 vs. CCR6 gating on Tfh cells from a representative healthy control and *PIK3R1* LOF patient. **(I and J)** Graphs show proportions of cells with a Th1 ($CXCR3^+CCR6^-$), $CXCR3^-CCR6^-$, Th17 ($CXCR3^-CCR6^+$), Th1/Th17 ($CXCR3^+CCR6^+$) phenotype within the (I) non-Tfh memory and (J) Tfh populations in controls and *PIK3R1* LOF patients. **(K)** The proportion of total natural killer (NK) cells and CD56 bright and CD56 dim NK cells. Each point represents a different individual, bars give mean ± SEM. Statistical significance was determined by Mann–Whitney test except G, which used a Kruskal–Wallis test, *P < 0.05, **P < 0.01, ***P < 0.001, ****P < 0.0001. Source data are available for this figure: SourceData FS1.

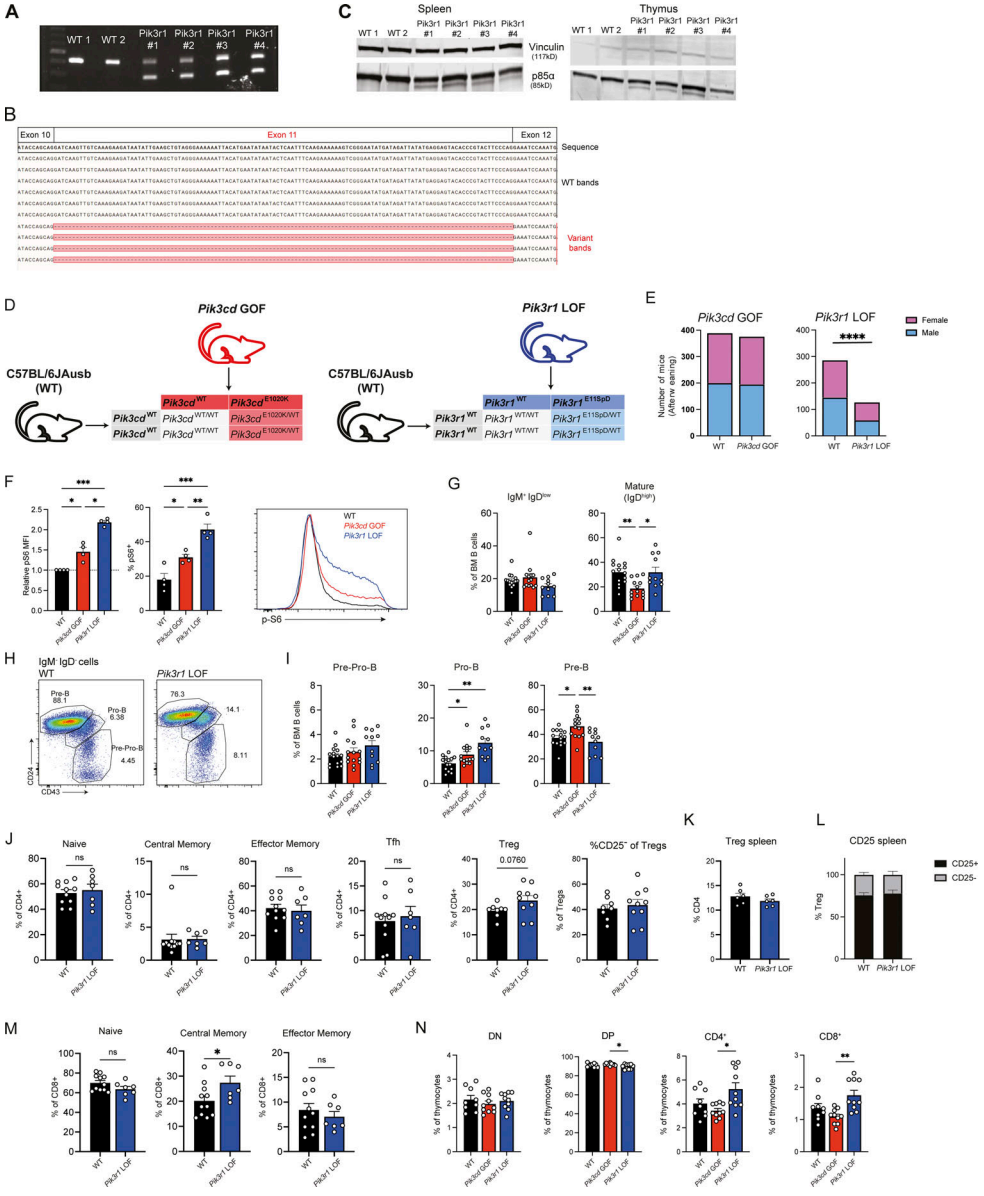

Figure S2. **Generation and analysis of *Pik3r1* LOF mice. (A)** PCR for exon 11 flanking region of *Pik3r1* was performed on cDNA from WT and *Pik3r1* LOF splenocytes. **(B)** Lower bands from *Pik3r1* LOF in A were sequenced to confirm deletion of exon 11. WT bands are shown for comparison. **(C)** Western blotting for p85α was performed on whole-cell lysates from WT and *Pik3r1* LOF splenocytes or thymus. Vinculin is included as a loading control. **(D–F)** Offspring from *Pik3cd* GOF breeding pairs and *Pik3r1* LOF breeding pairs were assessed for their genotype. **(D)** Setup of *Pik3cd* GOF and *Pik3r1* LOF breeding pairs and expected genotypes of offspring—a 1:1 ratio of WT:mutant offspring is expected. **(E)** Numbers of WT, *Pik3cd* GOF, and *Pik3r1* LOF offspring from their respective breeding pairs. Significant differences of observed versus expected were calculated using GraphPad Prism, ****P < 0.001. **(F)** Sorted follicular B cells were intracellularly stained for phosphorylated S6 at a resting state. Graphs show pS6 mean fluoresence intensity (MFI) normalized to WT levels, or % pS6$^+$ cells for each genotype. Each point represents B cells isolated from a separate mouse, bars give mean ± SEM, *n* = 4. Histograms show representative expression of p-S6. **(G–I)** BM from young (9–12 wk) WT, *Pik3cd* GOF, and *Pik3r1* LOF mice were stained to identify different B cell populations by flow cytometric analysis. **(G)** Percentages of IgM$^+$ IgD^{low}, IgD^{high}, and IgM$^-$ IgD$^-$ B cells. **(H and I)** Representative pseudocolor plots gated on IgM$^-$ IgD$^-$ cells and percentages of pre-pro (CD43^{high} CD24^{low}), pro (CD43^{mid} CD24^{high}), and pre (CD43^{low} CD24^{high}) B cells. Graphs in G–I show mean ± SEM, each point represents a different animal, *n* = 10–15 per group. Significant differences were determined by one-way ANOVA, *P < 0.05, **P < 0.01, ***P < 0.001. **(J)** Spleens from old (30–45 wk) WT and *Pik3r1* LOF mice were stained to identify different lymphocyte populations by flow cytometric analysis. Percentages of naïve, central memory, effector memory, Tfh (*n* = 11 WT, 7 *Pik3r1* LOF), and Treg CD4$^+$T cells (mean ± SEM, *n* = 8 WT, 10 *Pik3r1* LOF); each point represents a different animal; mean ± SEM are shown in bar graphs. **(K–M)** Spleens from young (9–12 wk) WT and *Pik3r1* LOF mice were stained to identify Treg population (CD4$^+$FoxP3$^+$) or CD8$^+$ T cells by flow cytometric analysis. **(K)** Frequencies of Tregs within CD4$^+$T cells are shown. **(L)** Frequency of CD25$^+$ and CD25$^-$ Treg populations are depicted in the graph. Graphs in show mean ± SEM, *n* = 6 per group, each point represents a different animal. **(M)** Spleens from old (30–45 wk) WT and *Pik3r1* LOF mice were stained to identify different lymphocyte populations by flow cytometric analysis. Percentages of naïve, central memory, effector memory CD8$^+$T cells shown in bar graphs. Mean ± SEM, *n* = 7–11. Significant differences were determined by unpaired Students *t* tests, *P < 0.05. **(N)** Thymic development was assessed in young (9–12 wk) WT, *Pik3cd* GOF, and *Pik3r1* LOF mice. Bar graphs represent the frequencies of double negative (DN), double positive (DP), CD4$^+$ single positive, and CD8$^+$ single positive cells. Graphs show mean ± SEM, *n* = 9–10 per group. Significant differences were determined by one-way ANOVA, *P < 0.05, **P < 0.01. Source data are available for this figure: SourceData FS2.

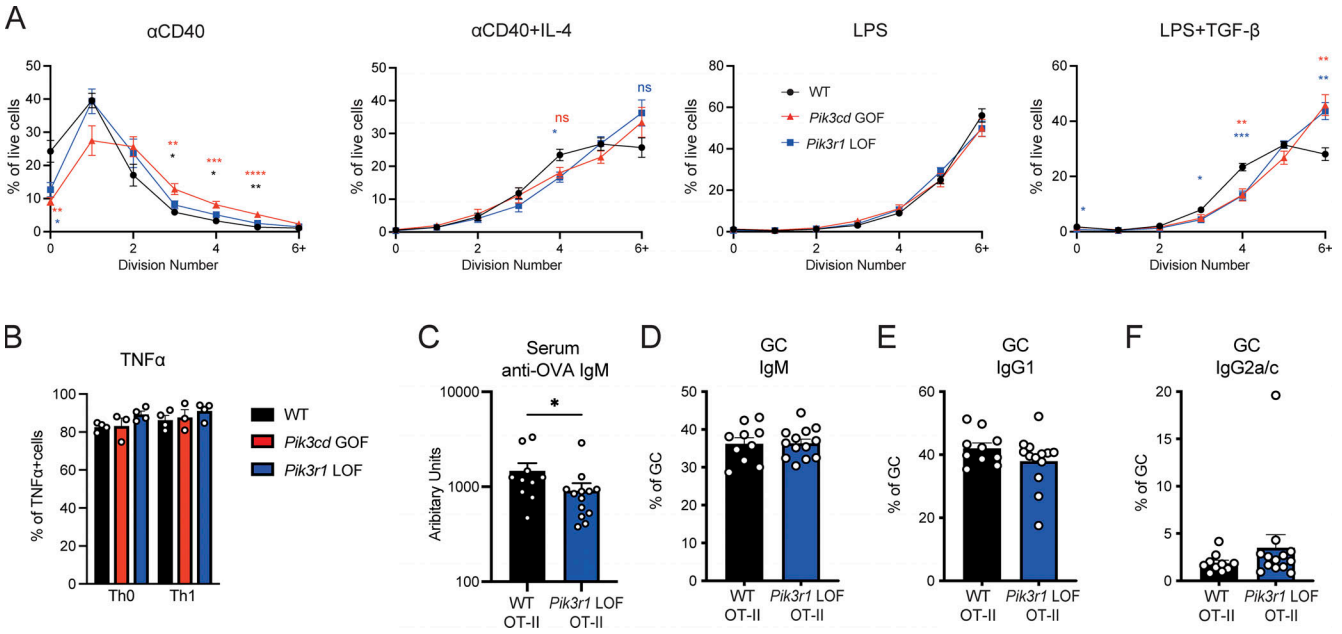

Figure S3. **Responses of *Pik3r1* LOF lymphocytes. (A)** Follicular B cells ($B220^+CD93^-CD21^{high}CD23^{high}$) were sorted from spleens of young (9–12 wk) WT, *Pik3cd* GOF, and *Pik3r1* LOF mice. Cells were labeled with CellTrace Yellow and then stimulated with αCD40+IL-4 or LPS + TGFβ for 4 d. Graphs show percentage of cells per division. All graphs show mean ± SEM from four independent experiments. Each experiment was performed using $n = 2$ pooled mouse spleens. Significant differences were determined by one-way ANOVA, *P < 0.05, **P < 0.01, ***P < 0.001, ****P < 0.0001. Significant differences between WT and *Pik3cd* GOF, WT and *Pik3r1* LOF, and *Pik3cd* GOF and *Pik3r1* LOF B cells are indicated in red, blue, and black, respectively. **(B)** Naïve $CD4^+$ T cells ($CD4^+CD44^{lo}CD62L^{hi}$) were sorted from spleens of WT, *Pik3cd* GOF, or *Pik3r1* LOF mice, stimulated with anti-CD3 and anti-CD28 mAbs under polarizing conditions for 4 d and then restimulated with PMA/ionomycin. Cells were harvested and stained for intracellular expression of TNFα. Graphs depict summary data of cytokine production under each condition stated under each graph. Significant differences were determined by ordinary one-way ANOVA. Plots show mean ± SEM from four independent experiments. **(C–F)** WT or *Pik3r1* LOF OT-II T cells were transferred into SAP^{KO} recipients, which were then immunized with OVA/Alum intraperitoneally. (C) Serum was collected and the level of anti-OVA IgM determined by ELISA. Expression of (D) IgM, (E) IgG1, and (F) IgG2a/c in GC B cells were measured through flow cytometry on day 7. Each point represents a different mouse, bars show mean ± SEM, $n = 10–13$. Significant differences were determined by Mann–Whitney, *P < 0.05.

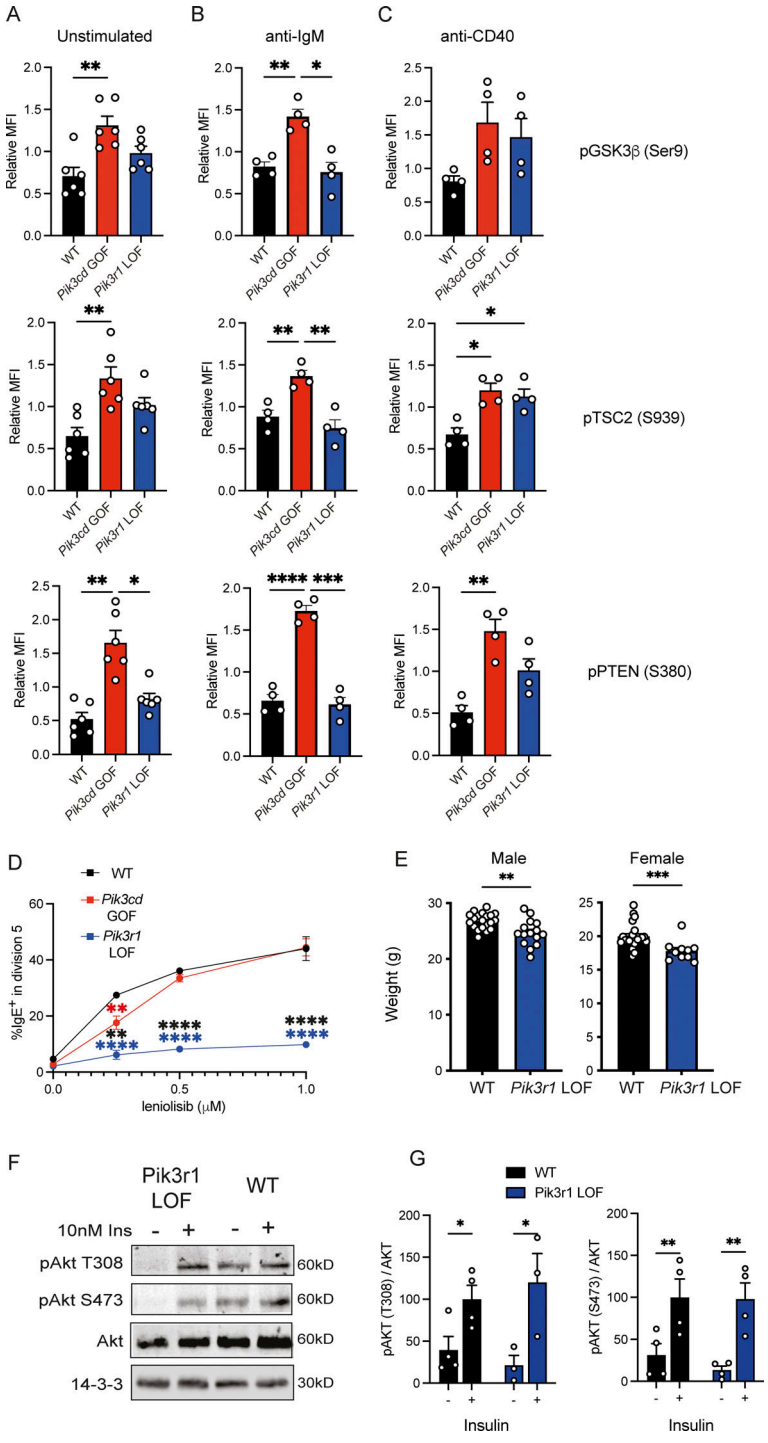

Figure S4. **Extended phenotyping of *Pik3r1* LOF mice. (A–D)** Follicular B cells (B220^{+}CD93^{-}CD21^{high}CD23^{high}) were sorted from spleens of WT, *Pik3cd* GOF, and *Pik3r1* LOF mice. **(A–C)** Cells were left unstimlated (A) or stimulated with αIg (B) or αCD40 (C) for 30 min. Total cell lysates were prepared and pGSK3β, pTSC2, and pPTEN was determined using the Milliplex MAP Total Akt/mTOR Magnetic Bead 11-Plex Kit. Values were normalized to mean values for each experiment. Each point represents an individual sorted B cell population from different mice, from at least three independent experiments, bars give mean ± SEM, *n* = 4–6. Significant differences were calculated by one-way ANOVA. **(D)** Cells were labeled with CellTrace Yellow and stimulated with αCD40+IL-4 for 4 d in the presence of DMSO (control) or various concentration of leniolisib as shown. Cells were then harvested and stained for IgE. The percentage of IgE^{+} switched cells in division 5 was plotted for each concentration of inhibitor. Graph shows mean ± SEM from two independent experiments. Significant differences were calculated by two-way ANOVA, **P < 0.01, ****P < 0.0001. **(E)** Mice were weighed at 9–10 wk of age. Each point indicates an individual animal, bars show mean ± SEM, male WT *n* = 20, *Pik3r1* LOF *n* = 15, female WT *n* = 23, *Pik3r1* LOF *n* = 10. Significant differences were determined by Mann–Whitney, **P < 0.01, ***P < 0.001. **(F and G)** Epidydimal white adipose explants from *Pik3r1* LOF and littermate WT control were treated with PBS or 10 nM insulin for 20 min. **(F)** Representative Western blot of protein expression for total Akt, phosphorylated Akt (pAkt T308 and pAkt S473), and loading control (14-3-3) in response to ±10 nM insulin. **(G)** Quantification of Western blots (F) of phosphorylated Akt (T308 and S473) normalized to total Akt levels. Each point represents a different mouse, bars represent means ± SEM (*n* = 3–4 animals per condition). Source data are available for this figure: SourceData FS4.

Provided online is Table S1, which shows *PIK3R1* LOF patient cohort clinical, genetic, and demographic information.